JOURNAL OF GEOPHYSICAL RESEARCH, VOL. 112, E08007, doi:10.1029/2006JE002803, 2007

Morphology and emplacement of a long channeled lava flow near Ascraeus Mons Volcano, Mars

W. Brent Garry,[1] James R. Zimbelman,[1] and Tracy K. P. Gregg[2]

Received 20 July 2006; revised 27 October 2006; accepted 27 February 2007; published 18 August 2007.

[1] Channeled lava flows, hundreds of kilometers long, are common on the lower flanks of the Tharsis Montes on Mars. Our analysis of a 690-km-long lava flow along the southwest perimeter of Ascraeus Mons shows that it was emplaced on low local slopes (<0.3°), with a deep channel (~20 m), and at high effusion rates (19,000–29,000 m^3/s) calculated from the Graetz number. These parameters are similar to conditions needed to yield rapidly emplaced terrestrial flows >100 km in length, but the maximum effusion rates necessary on Earth are essentially the minimum for Martian flows. On the basis of our calculated effusion rates, the eruption duration was 3 to 7 Earth months, assuming a constant effusion rate and continuous eruption. The morphology of the Ascraeus Mons flow shows similarities to terrestrial and simulated channeled flows. Downstream changes in morphology resemble those observed in the 1907 flow, Mauna Loa Volcano, Hawaii and channeled polyethylene glycol (PEG) flows. Braided sections of the channel in the Ascraeus Mons flow contain islands which are hundreds of meters across and resemble features observed in the 1907 and 1984 flows on Mauna Loa Volcano. Crosscutting relationships suggest islands in the proximal section were shaped by thermal and mechanical erosion, whereas islands in the medial section are inferred to be material rafted by surges of lava through the channel. Overall, understanding the morphology of long lava flows on Mars is essential to the interpretation of their emplacement and constraining eruption conditions in the saddle regions of the Tharsis volcanoes.

Citation: Garry, W. B., J. R. Zimbelman, and T. K. P. Gregg (2007), Morphology and emplacement of a long channeled lava flow near Ascraeus Mons Volcano, Mars, *J. Geophys. Res.*, *112*, E08007, doi:10.1029/2006JE002803.

1. Introduction

[2] Lava channels are common volcanic features and an efficient means of quickly transporting large volumes of material several kilometers, as documented for historic eruptions on Earth. For example, the Honokua flow traveled 24 km in 3 hours during the 1950 eruption of Mauna Loa Volcano, Hawaii [*Macdonald and Abbott*, 1970]. Channeled lava flows on Mars commonly extend tens to hundreds of kilometers and have been documented in the Tharsis and Elysium volcanic regions [e.g., *Zimbelman*, 1985, 1998; *Mouginis-Mark and Tatsumura-Yoshioka*, 1998; *Baloga et al.*, 2003]. The immense scale of these Martian flows surpasses the longest known channeled lava flows documented in historic eruptions on terrestrial subaerial volcanoes; for example, the ~51-km-long lava flow, 1859 eruption, Mauna Loa Volcano, Hawaii [cf. *Rowland and Walker*, 1990]. Terrestrial tube-fed compound flows as well as continental flood basalts are hundreds of kilometers long [e.g., *Atkinson et al.*, 1975; *Self et al.*, 1997], but these tend to form by the coalescence of lobes in broad flows or follow a preexisting valley rather than being confined within a narrow flow bounded by levees formed during emplacement. Despite their greater flow lengths, channeled lava flows on Mars have similar morphologic features to terrestrial lava channels [e.g., *Carr and Greeley*, 1980].

[3] Here, we document the morphology and emplacement parameters of a 690-km-long, channeled lava flow found in the topographic saddle between Ascraeus and Pavonis Montes on Mars (Figure 1) [*Zimbelman*, 1998], referred to herein as the Ascraeus Mons flow. Data from Mars Orbiter Laser Altimeter (MOLA) [*Smith et al.*, 1998], Mars Orbiter Camera (MOC) [*Malin et al.*, 1998], and the Thermal Emissions Imaging System (THEMIS) [*Christensen et al.*, 2004] are used to revise a preliminary analysis by *Zimbelman* [1998] that was based exclusively on Viking Orbiter (VO) data. High-resolution (≤32 m/pixel) images from MOC and THEMIS have revealed details that warrant further study of the flow (Table 1). Our goal is to analyze the morphology of the Ascraeus Mons flow, detail specific flow features, and interpret its emplacement.

[4] Ascraeus Mons, one of four large Tharsis volcanoes, measures 375 km wide, 870 km long, and 15 km high [*Plescia*, 2004]. Previous studies of Martian lava flows have focused on rheology and emplacement. *Zimbelman* [1985] analyzed Ascraeus Mons summit flows lavas from VO images and determined average yield strengths (2.1×10^4 Pa),

[1]Center for Earth and Planetary Studies, Smithsonian Institution, Washington DC, USA.
[2]Department of Geology, University at Buffalo, Buffalo, New York, USA.

0148-0227/07/2006JE002803$09.00

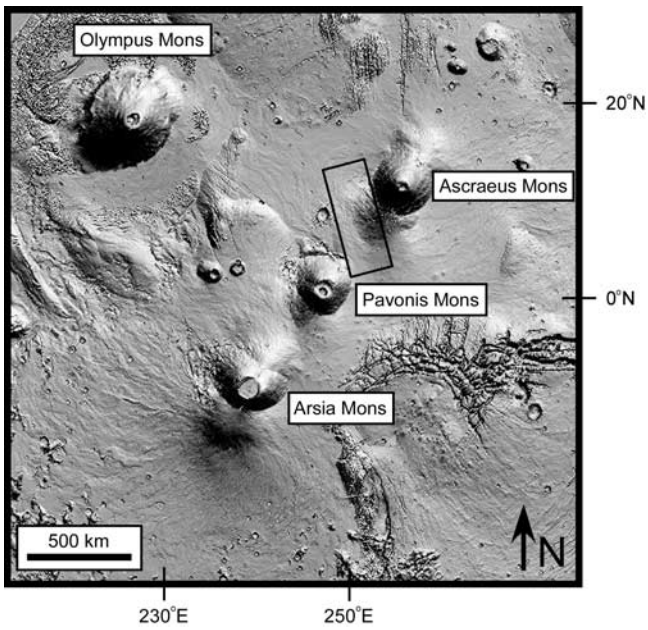

Figure 1. Shaded relief map of the Tharsis region on Mars. Box outlines location of the Ascraeus Mons lava flow. Map composed in Gridview [*Roark et al.*, 2000] with MOLA data gridded at 32 m/pixel.

effusion rates (35 m^3/s), and viscosities (2.3×10^4 Pa s) comparable to those of terrestrial basaltic to basaltic-andesite lavas. Those flows, which are 8–19 km long, are shorter than, and emplaced at a different location (summit versus saddle), from the Ascraeus Mons flow studied here. The viscosity of a nearby ~500-km-long lava flow originating from Pavonis Mons was determined to increase an order of magnitude along the distal 175 km of the flow [*Baloga et al.*, 2003]. Martian lava flows exhibit a greater increase in viscosity along the flow length and with time than in terrestrial flows for given eruption conditions [*Glaze and Baloga*, 1998]. *Rowland et al.* [2004] showed that flow lengths on Mars would be shorter than on Earth for a given volumetric flow rate and the respective environments for each planet based on results from the computer model FLOWGO [*Harris and Rowland*, 2001]. Therefore, when applying equations derived from, and originally applied to, terrestrial lava flows [cf. *Pinkerton and Wilson*, 1994] to Martian lava flows, results for effusion rates and emplacement durations will be minimum values. Dimensionally, Martian and terrestrial lava flows have the greatest fluctuations in flow width within the proximal section and exhibit a widening at the transition from the channeled to nonchanneled portion [*Peitersen and Crown*, 1999].

[5] We compare the Ascraeus Mons flow to: the Mana flows on Mauna Kea Volcano, Hawaii; the 1907 flow, Mauna Loa Volcano, Hawaii; and a series of channeled polyethylene glycol (PEG) flows with respect to overall flow morphology, flow thickness, and island structures within the channel. The field work by Zimbelman and others between 2004 and 2006 has been used to constrain the emplacement parameters of the two Hawaiian flows and the potential eruption hazards for residents living along Mauna Loa's southwest rift zone (J. R. Zimbelman, W. B. Garry, A. K. Johnston, and S. H. Williams, Precision topography applied to an evaluation of the emplacement of the 1907 Mauna Lao basalt flow, Hawaii, in review, *Journal of Volcanology and Geothermal Research*, hereinafter referred to as Zimbelman et al., in review). A Trimble R8 Differential Global Positioning System (DGPS), consisting of a stationary base and roving receiver (horizontal accuracy: ~1–2 cm; vertical accuracy: 2–4 cm), was used to collect precise topographic data of the two Hawaiian lava flows. The 1907 flow erupted over a period of 15 days [*Barnard*, 1990; *Barnard*, 1995], covers an area of 25.1 km^2, and has an estimated volume of 86.6 million m^3 based on the mapping of IKONOS images (2 m/pixel) and flow thicknesses obtained from topographic surveys (Zimbelman et al., in review). The Mana flows are benmoreite a'a flows emplaced in the Pleistocene (65–14 ka) [*Wolfe and Morris*, 1996] on the north flank of Mauna Kea Volcano. The majority of the flows are covered by grass and several centimeters of soil, but outcrops do exist. On Mars, alkaline volcanic rocks are present in the Columbia Hills in Gusev Crater [*McSween et al.*, 2006].

[6] Researchers have used PEG extensively to simulate lava flows in subaerial, submarine, and extraterrestrial environments [e.g., *Fink and Griffiths*, 1990, 1998; *Griffiths and Fink*, 1992a, 1992b, 1997; *Gregg and Fink*, 1995, 1996, 2000; *Blake and Bruno*, 2000; *Griffiths et al.*, 2003; *Lyman et al.*, 2004; *Anderson et al.*, 2005; *Garry et al.*, 2006]. PEG is used for its dynamic properties and its temperature-dependent viscosity [*Fink and Griffiths*, 1990]. The various morphologies that form when PEG flows solidify resemble natural lava flow morphologies [e.g., *Fink and Griffiths*, 1990; *Gregg and Fink*, 1995, 2000; *Griffiths et al.*, 2003; *Garry et al.*, 2006]. Channeled PEG flows exhibit comparable physical and morphologic features to subaerial channeled flows [*Garry*, 2006]. We expect the downstream changes in flow width and channel width of the Ascraeus Mons flow to be similar to both channeled PEG flows and terrestrial flows even though they all have dramatically different length scales (centimeters to hundreds of kilometers).

[7] The laboratory setup used for the simulation of channeled flows is modeled after that of *Fink and Griffiths* [1990]. Simulations are conducted by pumping warmed (~22–26°C) PEG at a constant effusion rate (~4–6 mL/s) into a tank filled with a chilled (~6–12°C) sucrose solution. PEG solidifies at ~18.5–20.0°C. Effusion rate is constant during the experiment. Dye is added to the clear, colorless PEG to add visual contrast between liquid and solid material. The slope of the tank floor is adjustable, and the flows presented here were emplaced on slopes of 8° and 12°, which are conducive for channel formation in PEG flows. Though the PEG experiments were conducted on slopes steeper than observed in the volcanic plains surrounding Ascraeus Mons, the results are still qualitatively applicable to lava flows formed on lower slopes [*Gregg and Fink*, 2000], including the Ascraeus Mons flow. A wire mesh covers the tank floor to prevent slipping of the PEG on the Plexiglas surface. Flow length and width are constrained by the tank dimensions (70 cm long, 28 cm wide) and therefore limit the flow volume to <2000 mL. Durations for the experiments were <400 s.

2. Ascraeus Mons Lava Flow

[8] The flow we investigate here extends around the southwest perimeter of Ascraeus Mons (Figure 1) in an

Table 1. Image Coverage of the Ascraeus Mons Flow as of February 2007[a]

Number	Type	Image ID	Center Latitude	Center Longitude
		THEMIS		
1	IR	I01252011	7.43°N	249.56°E
2	IR	I02363007	12.77°N	249.11°E
3	IR	I02700002	5.75°N	249.17°E
4	IR	I03424002	11.54°N	250.26°E
5	IR	I04073006	2.48°N	253.38°E
6	IR	I04972005	6.25°N	248.89°E
7	IR	I06370030	9.30°N	252.77°E
8	IR	I06420021	10.83°N	250.78°E
9	IR	I07069019	5.50°N	253.58°E
10	IR	I07094019	5.39°N	252.61°E
11	IR	I07431020	−6.86°N	252.524°E
12	IR	I07456017	5.77°N	253.03°E
13	IR	I07531017	11.91°N	250.97°E
14	IR	I07818019	7.81°N	253.93°E
15	IR	I07843020	5.68°N	252.70°E
16	IR	I07868021	6.64°N	251.62°E
17	IR	I07893024	7.79°N	251.06°E
18	IR	I07943018	11.59°N	249.30°E
19	IR	I07968021	7.16°N	247.96°E
20	IR	I08230015	8.27°N	251.90°E
21	IR	I08692020	6.45°N	248.42°E
22	IR	I09603020	14.74°N	249.23°E
23	IR	I09478031	9.48°N	254.38°E
24	IR	I09890030	11.45°N	249.52°E
25	IR	I10489010	12.35°N	250.82°E
26	IR	I10726005	6.86°N	253.18°E
27	IR	I11425007	20.33°N	251.43°E
28	IR	I11974010	−0.084°N	251.580°E
29	IR	I15306008	3.492°N	254.142°E
30	IR	I15381008	5.25°N	250.63°E
31	IR	I16866021	2.462°N	252.752°E
32	IR	I16966011	4.963°N	248.408°E
33	IR	I17153014	11.333°N	254.807°E
34	IR	I17203011	10.643°N	252.383°E
35	IR	I17465023	−1.708°N	252.855°E
36	IR	I17515014	14.360°N	252.715°E
37	IR	I17565046	8.190°N	249.539°E
38	IR	I17877014	20.803°N	250.964°E
39	IR	I18114016	13.235°N	253.200°E
40	IR	I18139014	12.617°N	251.958°E
41	IR	I18476007	7.198°N	249.891°E
42	IR	I18688010	9.383°N	254.503°E
43	IR	I19025008	12.737°N	253.705°E
44	IR	I19412010	0.819°N	248.747°E
45	Visible	V02700003	8.285°N	249.79°E
46	Visible	V04972006	7.91°N	249.22°E
47	Visible	V08692021	9.95°N	249.00°E
48	Visible	V11138004	9.07°N	248.76°E
49	Visible	V11637009	4.43°N	253.47°E
50	Visible	V11712007	6.53°N	250.40°E
51	Visible	V11949008	3.67°N	253.08°E
52	Visible	V12311015	6.48°N	251.00°E
53	Visible	V12336009	5.86°N	249.58°E
54	Visible	V12648014	6.91°N	249.34°E
55	Visible	V13197007	5.14°N	252.35°E
56	Visible	V13484008	2.39°N	252.69°E
57	Visible	V14083011	5.14°N	253.76°E
58	Visible	V14445009	6.54°N	251.42°E
59	Visible	V14495018	7.34°N	249.19°E
60	Visible	V15980008	5.519°N	251.561°E
61	Visible	V15955011	4.842°N	252.628°E
62	Visible	V17852033	7.559°N	250.313°E
63	Visible	V19100049	11.793°N	250.155°E
64	Visible	V19100050	8.499°N	249.708°E
		MOC		
65	Visible	E12-02381	8.16°N	249.73°E
66	Visible	R14-01618	5.69°N	251.00°E
67	Visible	S05-00416	6.78°N	250.26°E
68	Visible	S05-00824	10.23°N	248.59°E
69	Visible	S06-00062	6.46°N	250.43°E
70	Visible	S07-00090	8.92°N	240.09°E
71	Visible	S07-01904	6.02°N	250.71°E
72	Visible	S07-02740	9.01°N	248.99°E
73	Visible	S08-01201	6.16°N	250.6°E
74	Visible	S08-02062	9.04°N	249.00°E
75	Visible	S09-00379	5.97°N	250.74°E
76	Visible	S09-01150	8.50°N	249.28°E
77	Visible	S10-00176	8.18°N	249.45°E

[a]THEMIS visible and IR images obtained from *THEMIS Public Data Releases* website http://themis-data.asu.edu. MOC images obtained from http://www.msss.com/moc_gallery/.

area mapped as intermediate-age Tharsis Montes flows, but the flow possibly originates from an area mapped as the youngest flows from Ascraeus Mons [*Scott et al.*, 1981]. The local underlying slope averages ~0.3°, measured in

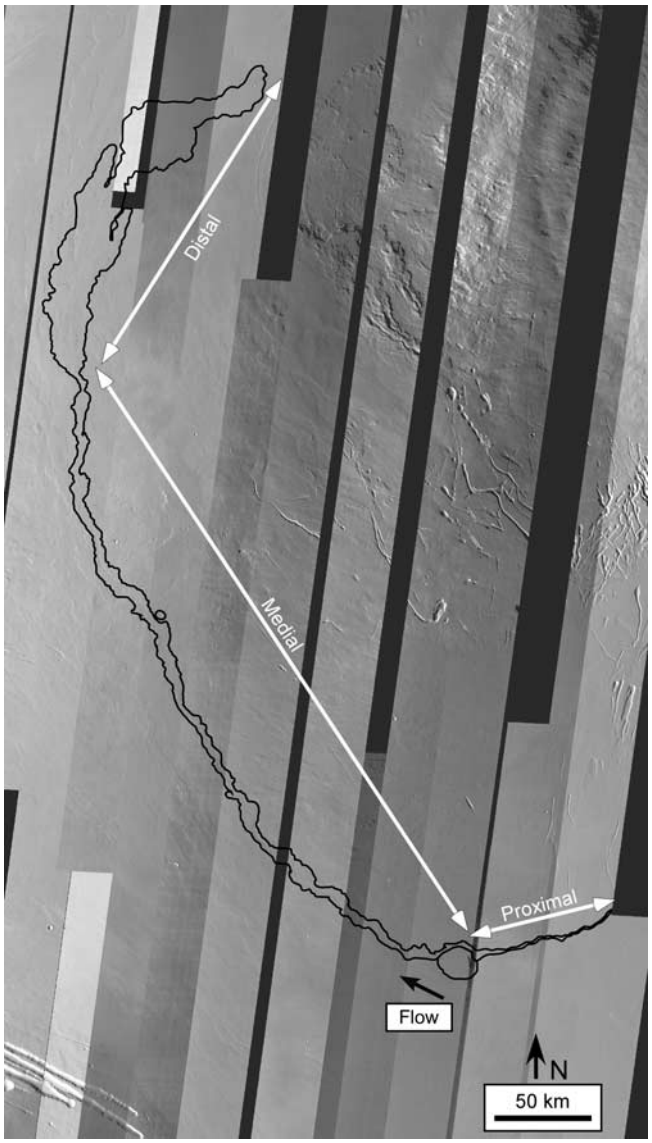

Figure 2. THEMIS daytime infrared (IR) mosaic of the Ascraeus Mons flow. Flow margin outlined in black. Proximal, medial, and distal sections are marked by double arrows. THEMIS IR images were map-projected in ISIS.

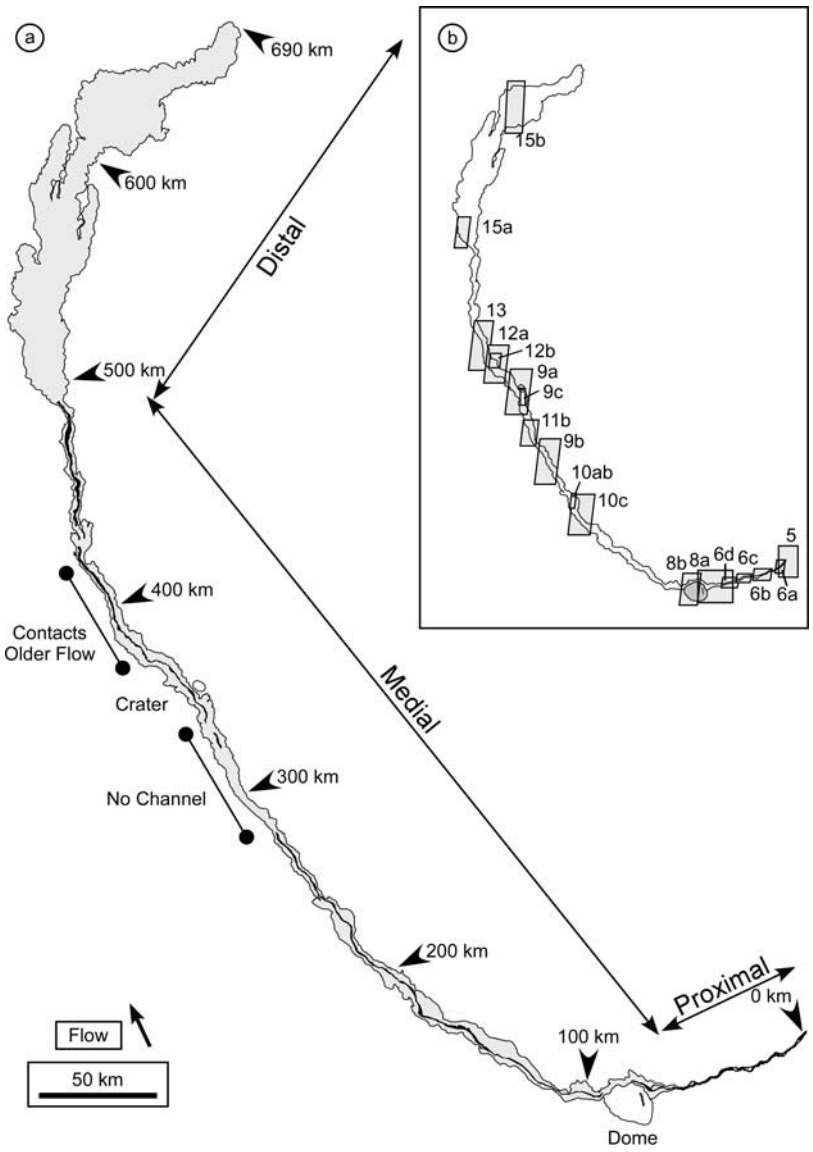

Figure 3. (a) Flow margin and channel outlines of the Ascraeus Mons flow. Flow sections (proximal, medial, distal), distances from the source, and previous topography (dome, crater) are labeled. Outline is of a mosaic of non map-projected THEMIS daytime infrared images. (b) Locations of THEMIS and MOC images listed by figure number.

Gridview [e.g., *Roark et al.*, 2000], an IDL-based program, using MOLA gridded data (128 pixels/degree). A mosaic of THEMIS daytime infrared (IR) images [*Christensen et al.*, 2006] provides a view of the entire flow at a resolution of 100 m/pixel (Table 1 and Figure 2). Each THEMIS daytime IR image was processed and projected using the Integrated Software for Images and Spectrometers (ISIS) [e.g., *Torson and Becker*, 1997; *Gaddis et al.*, 1997; *Anderson et al.*, 2004] from the U.S. Geological Survey. A map of the flow is presented in Figure 3a. Surface details of the channel and levees are observed in MOC images (4.5–6.5 m/pixel) and THEMIS visible images (19 m/pixel) (Figure 3b). Flow thicknesses were measured in topographic cross sections and from shadow measurements. All topographic cross sections are perpendicular to flow direction and were created in Gridview. We refer to the flow in three sections as follows: proximal, medial, and distal (Figures 2, 3, and 4). Each section boundary is characterized by a noticeable change in morphology. We define the entire Ascraeus Mons lava flow as the ''flow,'' the central conduit as the ''channel,'' and the entire width of material that bound the channel as ''levees.'' The levees and flow margins (for example, left and right levee) are referenced with respect to the observer looking downstream. Overall, the Ascraeus Mons flow is narrow ($\leq$10 km wide) with a central channel that transitions to a broad ($\leq$39 km wide) nonchanneled flow lobe distally (Figures 2, 3, and 4). The distal zone is situated within a prominent fan-shaped flow field. We focus on the Ascraeus Mons flow because the channel and flow margins are traceable over a considerable distance of the flow length. Additional channeled flows are observed adjacent to the Ascraeus Mons flow, but only portions of these flows are

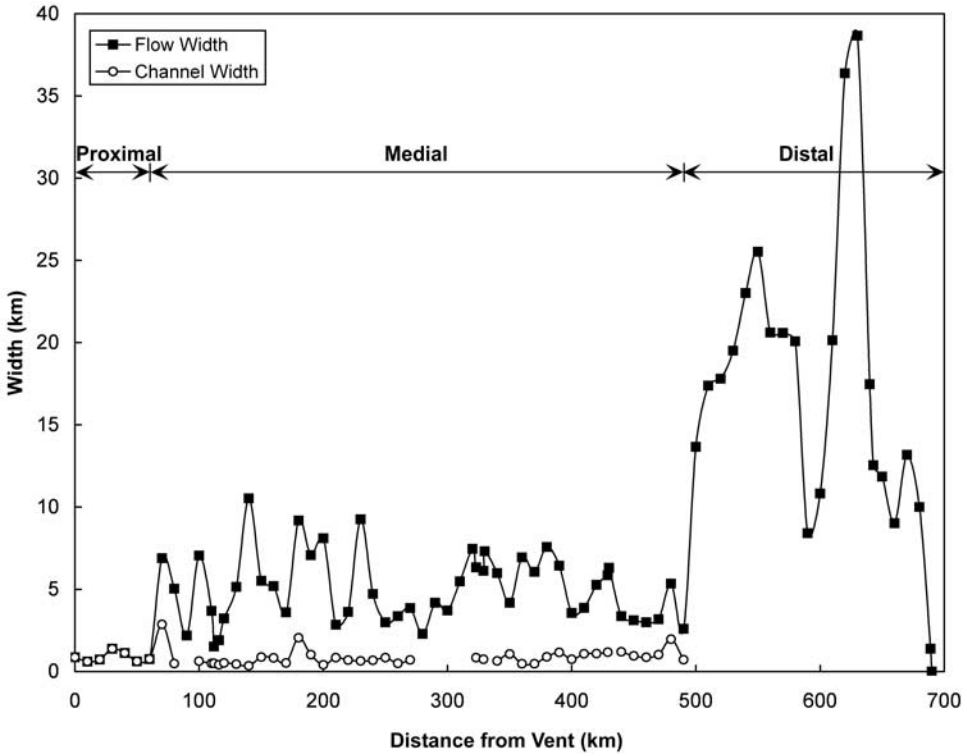

Figure 4. Downstream change in flow width and channel width with distance from the vent for the Ascraeus Mons flow.

visible. Further investigation of similar long flows in the Tharsis region is warranted for a comparative analysis of the emplacement of long lava flows on Mars.

2.1. Flow Dimensions

[9] The total measured flow length is ~690 km (Table 2), of which 444 km are channeled. The revised mapping of the flow margins yields a flow length 210 km greater than that mapped by *Zimbelman* [1998]. This flow length is a minimum because the exact location of the vent has not yet been identified, but is suspected to be along the saddle region between Ascraeus and Pavonis Montes. The uppermost part of the channel ends abruptly as observed in THEMIS IR image I18688010 (Figure 5). This indicates that the source area for the channel may have been roofed over during the eruption or covered by a younger flow. We do not see any evidence that the source of the Ascraeus Mons flow is related to a channel that terminates at the same juncture, but whose flow direction trends nearly perpendicular to the Ascraeus Mons flow. Flow widths and channel widths are measured at 10-km intervals (Figure 4). Flow width ranges from 0.6–38.6 km, with an average of 8.0 km (±7.6). The channel width spans 0.3–2.9 km, but is typically <1.0 km (±0.5). The widths of the levees vary between 0.3–6.2 km, and average ~2.1 km (Table 2). Topographic cross sections from MOLA gridded data reveal flow thicknesses ≤115 m, whereas shadow measurements of the flow margin in the medial section of the flow yield thicknesses of 32–66 m (Table 3). These agree with flow thicknesses of 30–100 m calculated from shadow measurements of VO images [*Zimbelman*, 1998]. The flow covers an area of ~6200 km^2 and, assuming an average flow thickness of 50 m, has an estimated volume of ~310 km^3 (Table 2).

2.2. Flow Morphology

2.2.1. Proximal Section: 0–70 km

[10] The upstream portion of the Ascraeus Mons flow is defined by a channel with no distinguishable levees or flow margins (Figure 6). The channel ranges in width from 0.2 to 2.2 km along the first 70 km (Figure 4), with depths of 11 to 35 m based on shadow measurements and topographic cross sections (Table 3 and Figure 7). A nested channel, ~100 to 300 m wide, is present along the centerline of the primary channel for ~20 km of the flow length (Figures 6c and 6d). Adjacent to the primary channel is a ridge, 0.20 to 0.25 km wide, that is prominent along the left channel margin (Figure 6). A MOLA cross section indicates a topographic ridge on both margins of the channel (Figure 7b). The

Table 2. Flow Dimensions, Ascraeus Mons Flow, Mars

Parameter		Units	
Flow Width	W_F	km	0.6–38.6
Channel Width	W_C	km	0.3–2.9
Levee Width	W_L	km	0.3–6.2
Flow Thickness	H_F	km	0.02–0.11
Minimum Flow Length	L_F	km	690
Area	A	km^2	6200
Volume[a]	V	km^3	310

[a]Flow thickness of 50 m was multiplied by the area.

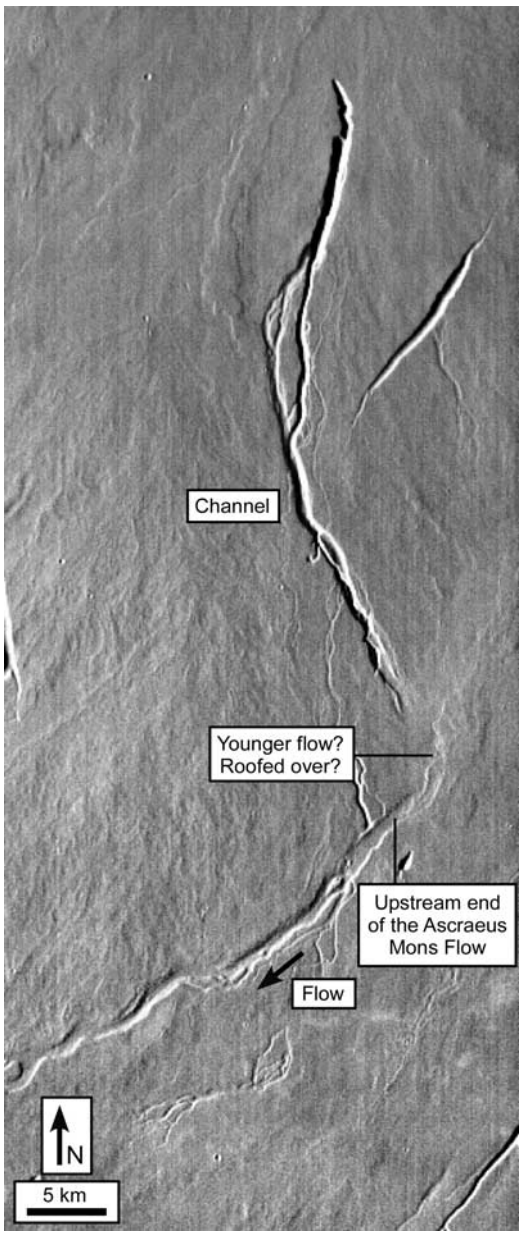

Figure 5. The uppermost portion of the Ascraeus Mons flow is traced upstream to a juncture with a thick flow and another channel perpendicular to the flow direction of the Ascraeus Mons flow, which is confined in the graben at the lower left of the image. THEMIS infrared image I18688010 (100 m/pixel).

"islands" that define the braided sections are oval and teardrop-shaped, 0.3 to 3.0 km in length, 0.2 to 1.0 km wide, and ~10 to 20 m in relief (Table 3). A complex relationship between the primary channel and local rivulets is observed (Figure 6a). The primary channel crosscuts rivulets oriented oblique to the flow direction, whereas a section of a narrow (<100 m) rivulet bisects an island within the channel.

[11] A dome, 16 by 31 km wide and ~70 m tall with a summit crack 5 km long and 650 m wide, marks the boundary between the proximal and medial sections. The flow width increases abruptly to ~2.9 km as the flow approaches the dome structure (Figures 3, 4, and 8a), and the channel and levees are observed along the dome's northern perimeter in both topographic cross section and a THEMIS visible image (Figures 7c and 8b).

2.2.2. Medial Section: ~70–500 km

[12] Downstream of the dome, the Ascraeus Mons flow is characterized by a well-defined channel, flow margin, and levees (Figure 9). Texturally, the channel appears as a monotone shade of gray and has a relatively featureless surface at these resolutions, on the basis of lack of shadows (Figure 9c). In contrast, the levees in the medial section are interspersed with topographically high materials (we refer to these as mounds) that are 12 to 19 m long and have a relief of 20 to 30 m, on the basis of shadow measurements (Table 3 and Figure 9c). Aeolian processes are evident from wind streaks and dunes. Superposition by aeolian deposits obscures some of the natural flow features. The channel is commonly <1 km wide, and the flow ranges in width from 1.5 to 10.5 km (Figure 4). Increases in channel width correspond to the presence of islands in the channel (Figure 10). These islands are 45 to 100 m in relief, comparable to thickness measurements of the flow margin (Table 3). The channel is not apparent along ~48 km of the flow length, except in a 7-km-long interval where it reappears (Figures 3a and 4). The distinct disappearance and reappearance of the channel are observed in THEMIS visible images (Figure 9). A THEMIS visible image (Figure 11b) and a topographic cross section (Figure 11c) of the apparent nonchanneled portion do not indicate the presence of a central channel. Shadows indicate that the flow is definitely thickened where the channel should be located (Figure 11b). The extensive widening of the right levee suggests that the Ascraeus Mons flow diverted around a preexisting crater (Figure 10a), and the confinement of the left flow margin by an older lava flow is also observed (Figures 11d, 12a, and 13). Channel width is very erratic in the section of flow past the crater, fluctuating between 0.2 and 1.0 km (Figure 12a).

2.2.3. Distal Section: ~500–690 km

[13] The lack of channel and an abrupt increase in flow width define the distal 190 km of the Ascraeus Mons flow (Figures 2, 3, and 4). The flow ranges in width from 8 to 39 km (Figure 4), and in thickness from 30 to 115 m (Figure 14), whereas shadow measurements yield flow thicknesses of 26 to 45 m (Table 3). The left margin of the Ascraeus Mons flow may have been influenced by an older, adjacent flow (Figure 14c). Ridges, 28 to 54 m high (Table 3), present at the transition from the medial to the distal section (Figure 15a) are inferred to reflect margins of individual lobes. Parallel, linear ridges define a preferred pathway 1.5 to 3.5 km wide, but not a consistent channel along the length of the distal section (bottom of Figure 15b).

3. Morphologic Analogs

3.1. Downstream Changes in Flow Dimensions

[14] Ten topographic DGPS profiles across the eastern lobe of the 1907 Mauna Loa flow reveal a downstream increase in both flow width (200 to 510 m) and channel

Table 3. Shadow Measurements From MOC and THEMIS Images

Image ID	Sun Azimuth, n°	Incidence Angle, n°	Theta (θ), n°	Flow Feature	Shadow Length, m	Height, m	
Proximal							
THEMIS V11637009	200	74.7	15.3	Island	40	11	
				Island	80	22	
				Channel Margin	80	22	
				Channel Margin	128	35	
THEMIS V11949008	201.4	76.2	13.8	Island	46	11	
				Channel Margin	80	20	
Medial							
MOC R14-01618	340.0	24.7	65.3	Island	40	87	A
				Island	45	98	B
				Island	27	59	C
MOC E12-02381	307.7	31.9	58.1	Mound	12	20	
				Mound	13	20	
				Mound	15	24	
				Mound	19	30	
				Mound	12	20	
THEMIS V02700003	192.7	60.1	29.9	Flow margin	69	40	M1
				Flow margin	114	66	M2
				Flow margin	56	32	M3
				Flow margin	74	43	M4
				Flow margin	77	44	M5
				Island	96	55	I1
				Island	114	66	I2
				Island	78	45	I3
				Island	97	56	I4
				Island	77	44	I5
				Channel margin	136	78	RL1
				Channel margin	78	45	LL1
				Channel margin	96	55	LL2
				Channel margin	115	66	LL3
Distal							
THEMIS V08692021	151.2	69.3	20.7	Ridge	110	41	
				Ridge	89	34	
				Ridge	143	54	
				Ridge	73	28	
				Ridge	106	40	
THEMIS V11737008	198.5	73.1	17.0	Margin	84	26	
				Margin	119	36	
				Margin	149	45	
				Margin	129	39	

width (15 to 222 m) (Zimbelman et al., in review). The DGPS profiles and corresponding IKONOS images indicate a prominent single channel in the proximal section of the eastern lobe which bifurcates into overlapping limbs in the medial section. The character of the levees changes from a smoothed, almost frothy pahoehoe surface with near vertical channel walls in the proximal section to a sequence of deformation levees composed of a'a in the medial section. The channel diffuses into a series of radial lobes at the flow front.

[15] Channeled PEG flows show a similar transition in morphology. The width of the flow, channel, and levees were measured at 2-cm intervals in still images of five PEG flows (Table 4 and Figure 16). Each image analyzed shows the flow at maximum flow length (70 cm), except for one flow (BG-97), which, at the time the image was taken and the vent was plugged, had only reached 60 cm. We observe the following trends in the graphs of the PEG flows: (1) Flow width near the vent remains constant or increases moderately, with a pronounced increase beginning ~20 cm downstream from the vent. (2) Fluctuations in channel width tend to mimic the increases or decreases in overall flow width. (3) Levees are narrower than the channel, except in one simulation (BG-97). (4) Levee width follows the following two main patterns: Fluctuations in levee width mimic each other (for example, increase in left levee and right levee width) or are opposite (for example, decrease in left levee when there is an increase in right levee). We recognize that the PEG experiments are conducted at constant flow rates and on constant underlying slopes for a short duration. Eruptions of natural flows experience fluctuations in effusion rate [e.g., *Wadge*, 1981; *Lipman and Banks*, 1987], changes in underlying slope, and variable topography (for example, hills, valleys).

3.2. Flow Thickness

[16] Two limbs of the Mana flow contrast in final flow morphology (Figure 17a). The western limb (Figure 17a) has rolling surface folds with a wavelength of ~50 m and the level of material in the channel is similar to the levee height, whereas the eastern lobe has highstanding levees and a low-lying channel floor. Levees in the eastern limb are 30 to 35 m thick, the channel is 120 m wide, and the flow is 425 m wide (Figure 17c and 17d) measured from DGPS profiles. Minimum thickness values for the Ascraeus Mons flow are comparable to the maximum thickness as measured

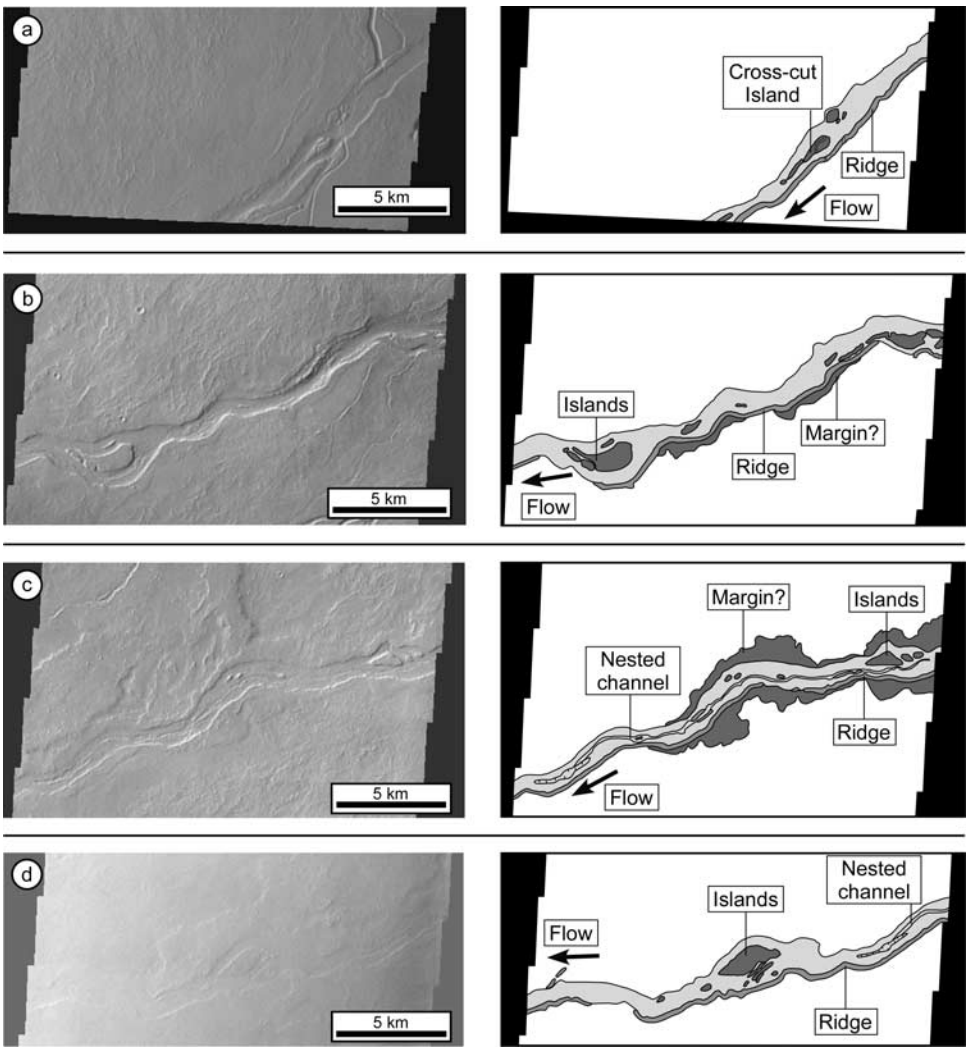

Figure 6. Images and corresponding flow maps of the proximal section of the Ascraeus Mons flow: (a) THEMIS visible image V14083011 (19 m/pixel), (b) THEMIS visible image V11637009 (19 m/pixel), (c) THEMIS visible image V11949008 (19 m/pixel), (d) THEMIS visible image V13484008 (19 m/pixel). Scale bars apply to both image and flow map.

on the Mana flow. In contrast, flow width and channel width are drastically different for the two flows; however, the Mana flow demonstrates that levee heights of tens of meters are possible for terrestrial, silica-poor lava flows.

3.3. Channel Islands

[17] Island features observed in the IKONOS images were documented in the field because they resemble similar features observed in the Ascraeus Mons flow. One of the islands is ~50 m long, 20 m wide, and 5–15 m in height, on the basis of DGPS topographic profiles (Figure 18). The plan view shape is oblong with the major axis parallel to flow. The material at the top of the island is dominantly a'a, while the sides of the island appear to have been "smoothed over." A linear "scar" parallel to flow direction, ~30 cm wide and ~3 m long, probably caused by solid material scraping the side of the island, indicates that the level of the lava in the channel was near the top of the island. A'a material has been built up along the margins of the top of the island, creating a central low that has entrapped a lava ball ~2 m in diameter. Islands were also observed in the 1984 flow on Mauna Loa Volcano and are associated with surge events of lava flowing down the channel. A mass of material is deposited as the surge wanes and is later streamlined by the flowing lava in the channel (J. Fink, personal communication, 2006).

4. Discussion

4.1. Flow Morphology

[18] The changes in morphology along the length of the Ascraeus Mons flow are consistent with changes observed in channeled terrestrial, Martian, and PEG flows [*Lipman and Banks*, 1987; *Peitersen and Crown*, 1999; *Garry*, 2006]. Characteristics of the proximal zone in the Ascraeus Mons flow suggest a zone of stability with an established channel. The thickening of the flow in the medial section is consistent with a downstream change in rheology and a

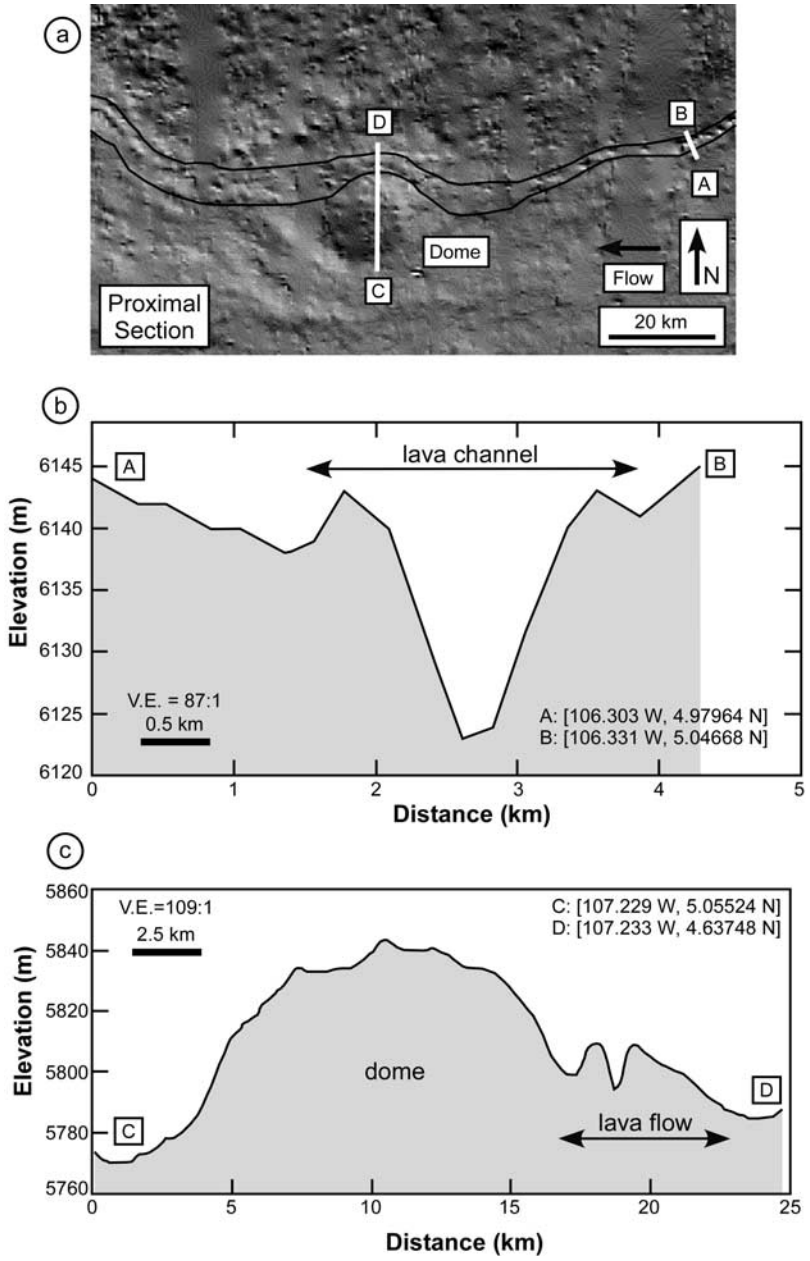

Figure 7. Map and topographic cross-sections of the proximal section created in Gridview. (a) Shaded relief map showing the area where the Ascraeus Mons flow passes the dome structure. Black lines outline the margins of the Ascraeus Mons flow. White lines mark locations of topographic cross sections. (b) Topographic cross section of the lava channel in the proximal section. V.E. is vertical exaggeration. Notice apparent ridges bordering the channel. (c) Topographic cross section showing the relation between the lava flow and the dome. Levees and channel are evident for the lava flow.

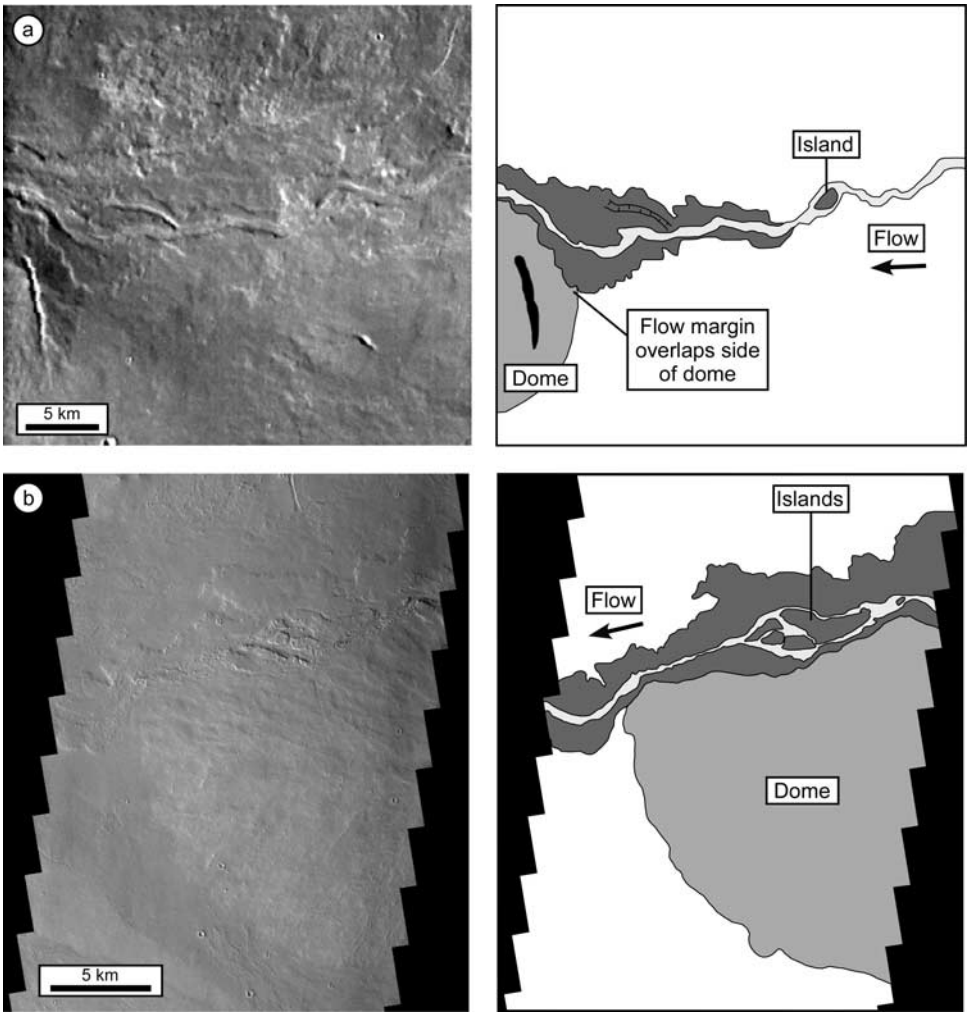

Figure 8. Images and flow maps of the Ascraeus Mons flow showing the interaction of the lava flow and the dome structure. (a) Margin of the lava flow overlaps the eastern portion of the dome. THEMIS infrared image I16866021 (100 m/pixel). (b) The Ascraeus Mons flow was diverted around the north side of the dome. The flow may have eroded a portion of the base of the dome. THEMIS visible image V15955011 (19 m/pixel).

response to previous topography, whereas the lack of channel formation in the distal section reflects a dispersed zone that we suggest is due to a decrease in flow velocity, increase in yield strength and viscosity, decrease in underlying slope, or a combination of these. The ~48-km-long nonchanneled zone in the medial section could have been produced by the following three different processes: (1) The channel roofed over as observed in the formation of pyroducts (lava tubes) [e.g., *Greeley*, 1987]; (2) late-stage lava stalled and solidified within the channel; or (3) a dam formed within the channel, causing the lava to back up.

[19] We interpret the island features in the proximal and medial section to have formed by different processes. Islands in the proximal section are thought to form by thermal and mechanical erosion and are discussed below. The islands in the medial section resemble the islands observed in channeled a'a flows on Mauna Loa Volcano. We infer that islands within the medial section of the Ascraeus Mons flow could have formed during surge events and are the remnants of material rafted downstream and eventually deposited within the channel based on observations by others of the 1984 flow and our observations of the 1907 flow on Mauna Loa Volcano. During the 1984 Mauna Loa eruption, formation of the islands in the channel coincided with surge events (*J. Fink*, personal communication, 2006). Channel crust, lava balls, and collapse of the levees can form dams within the channel, and surges form after lava breaks through these obstacles and the material is rafted downstream [*Lipman and Banks*, 1987]. The material is stranded within the channel as the flow velocity and level of the lava wane, and eventually, the deposit is eroded and streamlined by lava in the channel (*J. Fink*, personal communication, 2006). Islands in the channel of the 1907 flow also show evidence of streamlining along the sides, indicating that they were most likely formed by a similar process.

4.2. Estimates of Channel Velocity, Effusion Rate, and Duration

[20] We use standard equations for calculating the channel velocity and effusion rate for the Ascraeus Mons flow. Channel velocity (v_C) is calculated using the Jeffrey's

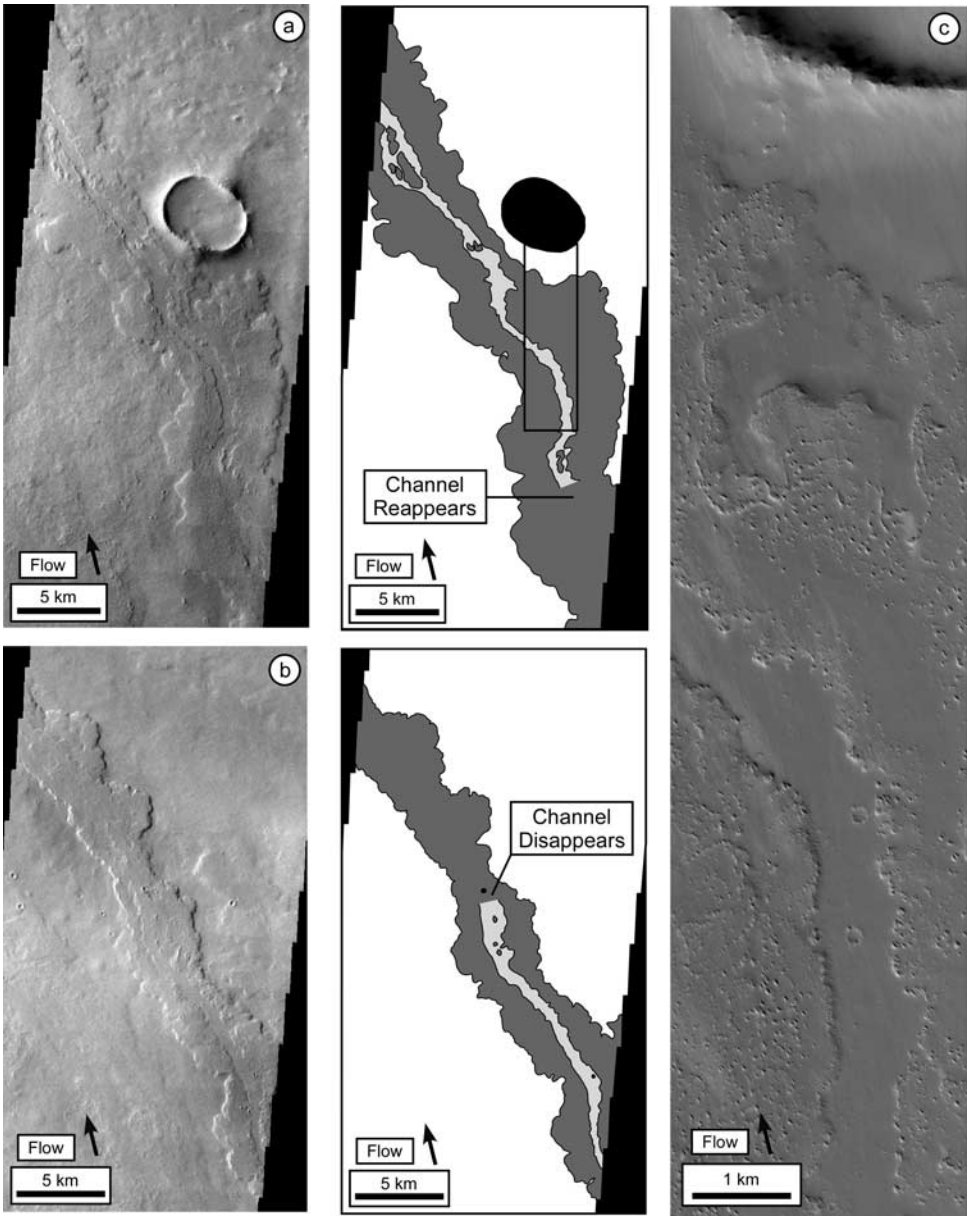

Figure 9. Images and flow maps of Figures 9a and 9b show where the lava channel disappears and reappears in the medial section of the Ascraeus Mons flow. (a) Reappearance of the channel. THEMIS visible image V12336009 (19 m/pixel). Box outlines location of adjacent MOC image. (b) Disappearance of the channel. THEMIS visible image V11712007 (19 m/pixel). (c) Surface textures of the channel and levees. MOC E12-02381 (4.60 m/pixel).

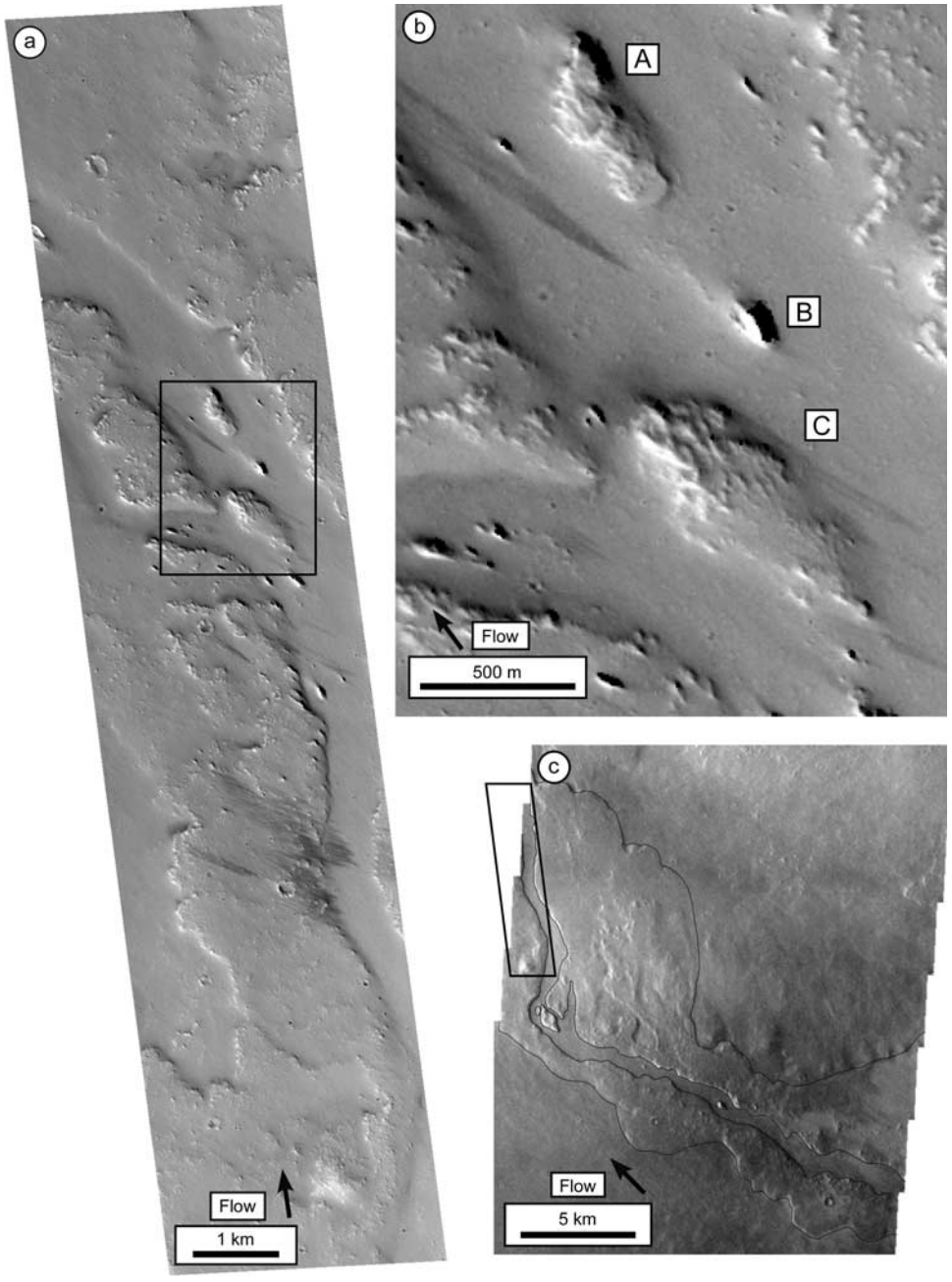

Figure 10. Island structures in the medial section of the Ascraeus Mons flow. (a) MOC R14-01618 (6.15 m/pixel). (b) Close-up of the islands shown in Figure 9a. Dimensions of these islands, labeled A, B, and C, are presented in Table 3. (c) Context image of the Ascraeus Mons flow. Box outlines location of MOC image shown in Figure 9a. THEMIS visible image V14445009 (19 m/pixel).

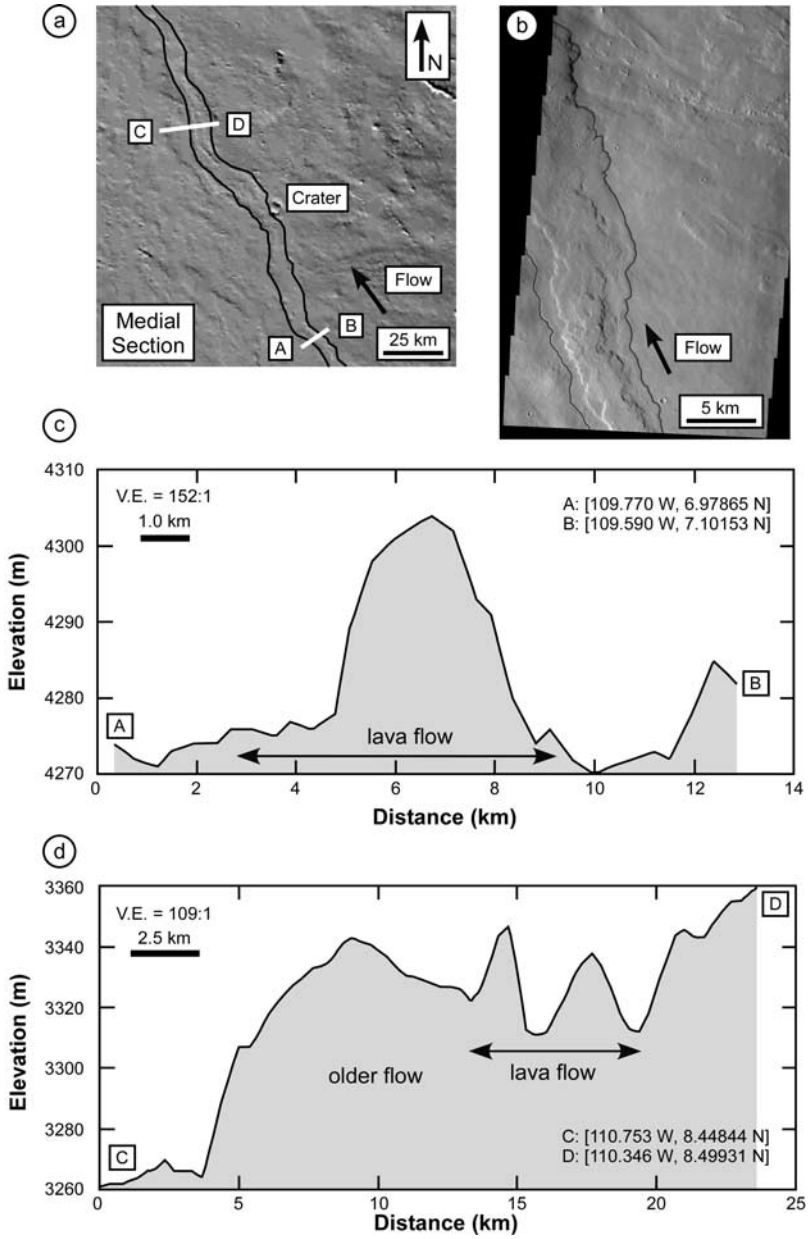

Figure 11. (a) Shaded relief map showing the area where the Ascraeus Mons flow is nonchanneled, passes the crater, and contacts an older lava flow. Map created in Gridview. White lines mark locations of the topographic cross sections. (b) Shadows indicate that the central part of the flow is covered by thick flow material which we interpret to be the cause for the nonchanneled part of the flow. THEMIS visible image V17852033 (19 m/pixel). (c) Topographic cross section of the nonchanneled part of the medial section. V.E. is vertical exaggeration. (d) Topographic cross section showing the relation between the lava flow and the adjacent older lava flow. Levees and channel are evident for the Ascraeus Mons flow in the cross section.

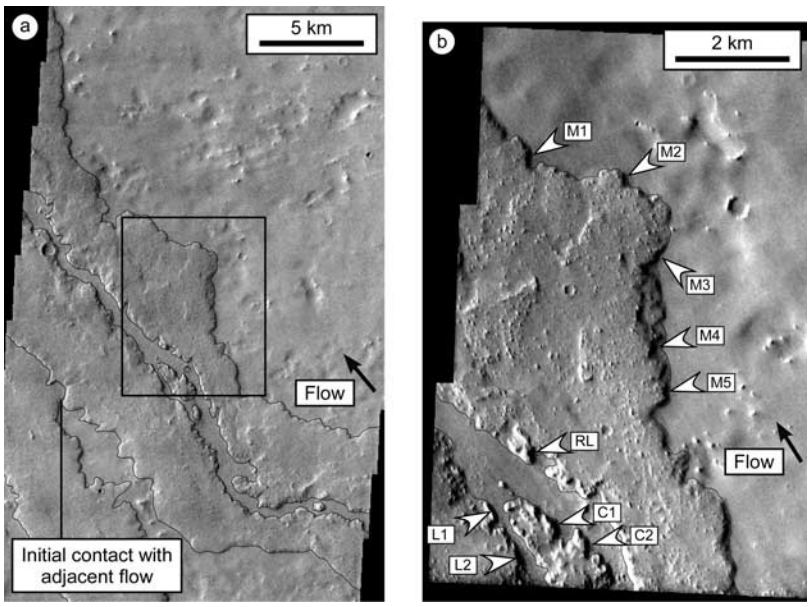

Figure 12. (a) Contact between the Ascraeus Mons flow and an adjacent lava flow. Black box outlines adjacent image. THEMIS Visible Image V12648014 (19 m/pixel). (b) Close-up of the channel and flow margin. Locations of shadow measurements are labeled (see Table 3). THEMIS visible image V02700003 (19 m/pixel).

equation [e.g., *Jeffreys*, 1925; *Fink and Zimbelman*, 1990; *Wilson and Mouginis-Mark*, 2001; *Rowland et al.*, 2004]:

$$v_C = \left(\rho_{lava}\, g_{Mars}\, d^2 \sin\theta\right)/(3\,\eta) \quad (1)$$

where ρ_{lava} is the density of the lava (2000–2600 kg/m^3), g_{Mars} is the acceleration due to gravity on Mars (3.7 m/s^2), θ is underlying slope (0.3°), d is channel depth (20 to 60 m), and η is the dynamic viscosity of the lava (10^3–10^5 Pa s). Our assumed values for density and dynamic viscosity are based on previous studies of channeled lava flows on Mars [e.g., *Zimbelman*, 1985; *Wilson and Mouginis-Mark*, 2001; *Baloga et al.*, 2003; *Rowland et al.*, 2004]. Equation (1) assumes a Newtonian rheology, laminar flow, and that the underlying slope and channel depth remain constant along the flow length; on the basis of observations of terrestrial basalt flows on the Hawaiian shields [e.g., *Lipman and Banks*, 1987], these are reasonable assumptions. We use channel depths of 20 to 60 m, which correspond to the flow margin thickness (Table 3) and channel depth in a topographic profile (Figure 7b). Channel velocities for the minimum assumed density (2000 kg/m^3) and viscosity (10^3 Pa s) values range from 5 to 46 m/s, with the higher velocities associated with deeper channel depths (Table 5). If we increase the assumed values for density (2600 kg/m^3) and viscosity (10^5 Pa s), the resulting channel velocities are lower (0.07 to 0.60 m/s). The calculated channel velocities for the Ascraeus Mons flow are similar to channel velocities of <1.0 to 17.8 m/s estimated for the 1984 flow on Mauna Loa with the upper limit observed in the vent region [*Lipman and Banks*, 1987; *Moore*, 1987; *Sakimoto and Gregg*, 2001]. Though the values for channel velocity are similar, we must note that the estimated channel depth for the 1984 flow is 2 to 7 m [*Lipman and Banks*, 1987], which is lower than our minimum estimate of channel depth for the Ascraeus Mons flow.

[21] The Reynolds number is used to determine if the style of flow is laminar or turbulent:

$$\mathrm{Re} = (\rho\, v_c\, d)/\eta \quad (2)$$

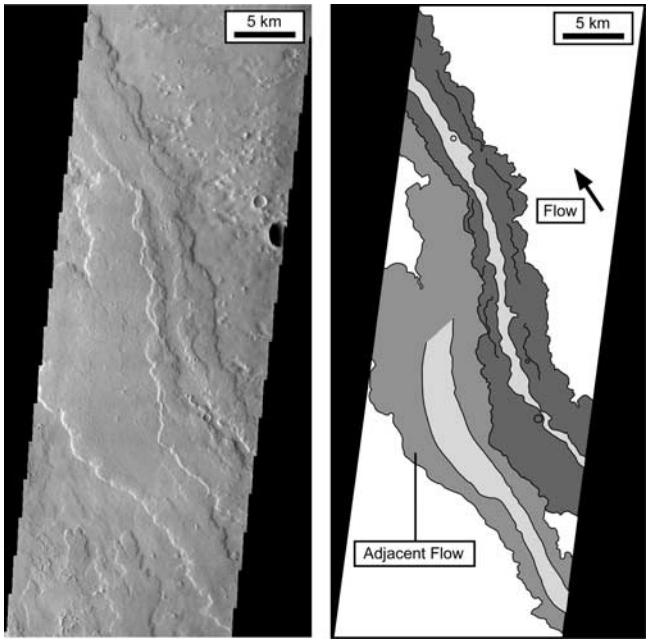

Figure 13. The Ascraeus Mons flow makes contact with an adjacent flow margin. THEMIS visible image V04972006 (19 m/pixel).

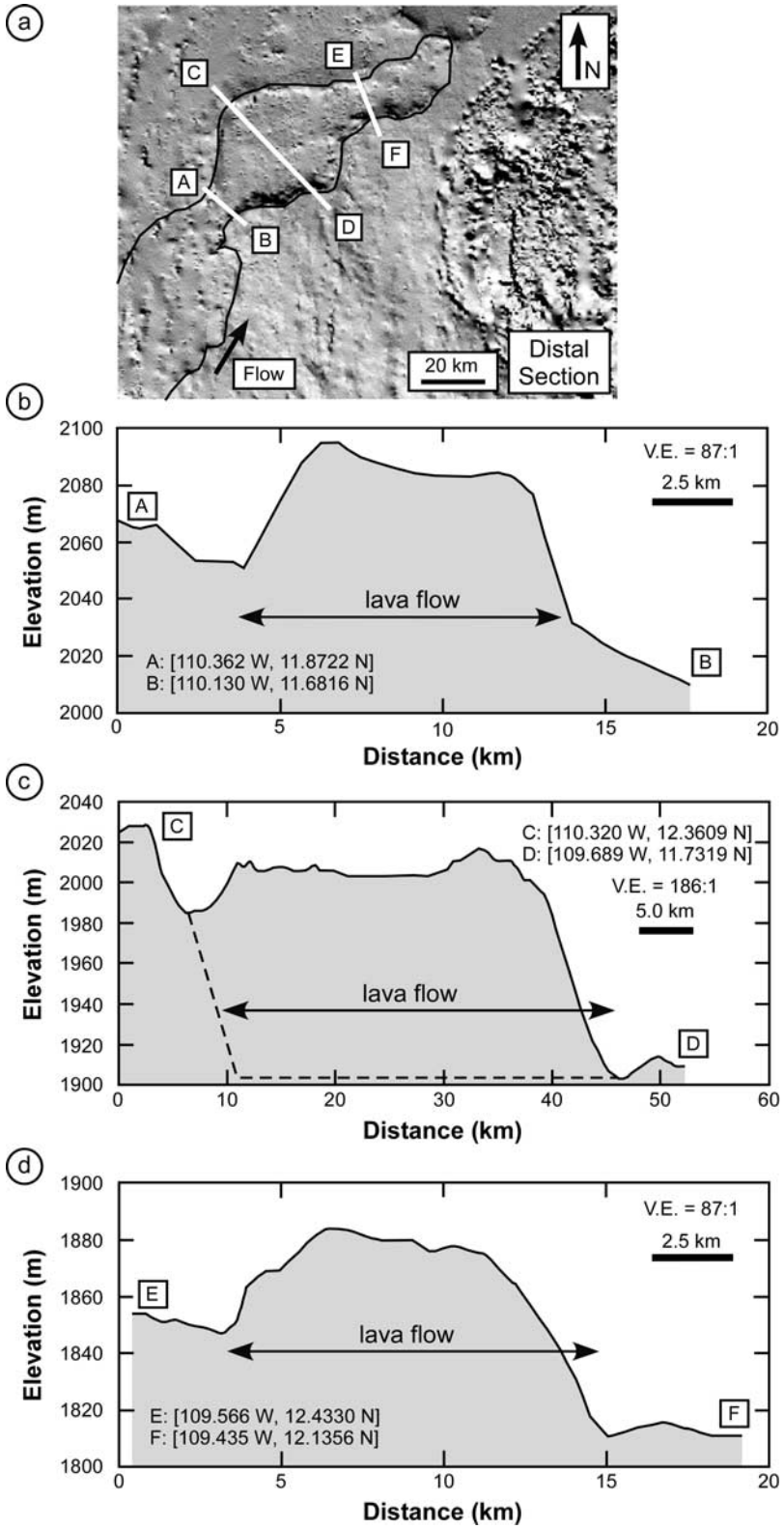

Figure 14. (a) Shaded relief map showing the distal end of the Ascraeus Mons flow. Map created in Gridview. White lines mark locations of topographic cross sections presented in Figures 14b, 14c, and 14d. Dashed line indicates hypothetical base of flow in Figure 14c.

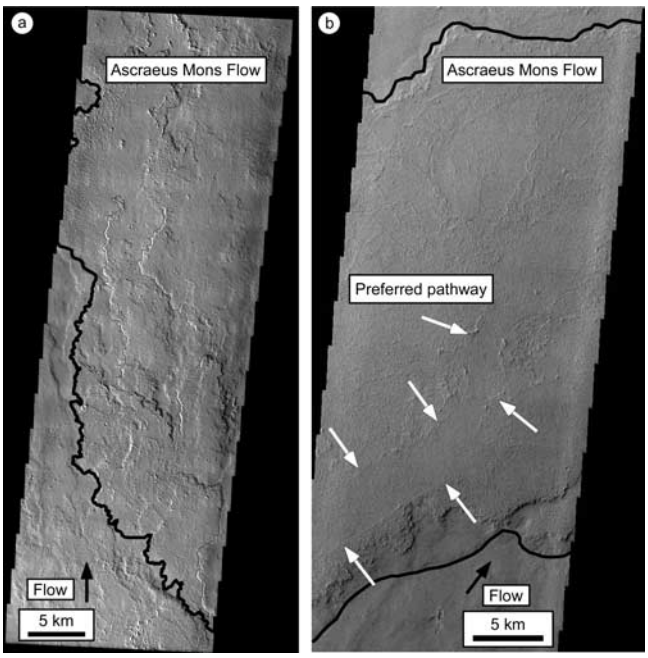

Figure 15. (a) Start of the distal section of the Ascraeus Mons flow. Black line marks the flow margin. Ridge orientations imply margins of overlapping lobes. THEMIS visible image V08692021 (19 m/pixel). (b) Parallel ridges bound a preferred pathway in the distal section. THEMIS visible image V11737008 (19 m/pixel).

with laminar flow corresponding to Re <2000. The emplacement of the Ascraeus Mons flow was dominantly laminar based on our calculations of Re using the values assumed above and calculated channel velocities (Table 5). The exception occurs with the lower density and dynamic viscosity values for channel depths of 50 and 60 m, where the Re values indicate turbulent flow. We feel that it is appropriate to disregard these values, because the lower density and viscosity values would most likely be associated with lava flowing through the proximal section of the flow, where channel depth is ~20 to 30 m. By the time lava has reached parts the medial section, assuming channel depth is equal to the observed flow thicknesses of 50 to 60 m, an increase in both density and viscosity would most likely have occurred [e.g., *Baloga et al.*, 2003] yielding Reynolds numbers in the laminar flow regime. Therefore we suggest that the Ascraeus Mons flow was emplaced by laminar flow, though turbulent flow may have occurred during surges of lava down the channel.

[22] We calculate the effusion rate by inverting the Graetz number (Gz) equation [*Hulme and Fielder*, 1977; *Wilson and Head*, 1983; *Pinkerton and Wilson*, 1994]:

$$Q = \mathrm{Gz}\,\kappa L W_F / h \tag{3}$$

where the Gz is assumed to be equal to 300 [*Pinkerton and Wilson*, 1994], κ is thermal diffusivity (7×10^{-7} m^2/s) [*Pinkerton and Wilson*, 1994], L is flow length, W_F is average flow width, and h is average flow thickness. Empirical studies of basaltic lava flows on Hawaii and Etna indicate that the lava flows would stop when the value of the Graetz number was equal to 300 and crust thickness was 1/3 the flow thickness [*Walker*, 1973; *Pinkerton and Sparks*, 1976; *Hulme and Fielder*, 1977; *Pinkerton and Wilson*, 1994]. The equation is applicable to Martian lava flows because the equation is dependent on properties of the lava flow and not on the environment. Equation (3) can be applied to flows of more silicic composition [*Pinkerton and Wilson*, 1994]; therefore, an assumption of a composition may not be critical. Use of the Graetz number assumes cooling-limited, laminar flow.

[23] Using an average flow width (8 km) and a range of flow heights (40 to 60 m) we calculate effusion rates between 1.9 and 2.9 $\times$ 10^4 m^3/s (Table 6). These values are considerably greater than the maximum effusion rate observed for the 1984 Mauna Loa eruption (~800 m^3/s) [*Lipman and Banks*, 1987] and estimations for the 1783–1784 Laki fissure eruption in Iceland (8700 m^3/s) [*Thordarson and Self*, 1993]. We calculated effusion rates of the 1984 Mauna Loa flow using equation (3) and published values of the final flow dimensions (L = 27 km, h = 7 and 10 m, W_F = 40, 50, and 60 m); these yield effusion rates of 23 to 49 m^3/s, which are 1 to 2 orders less than initial eruption values. These results correlate with minimum effusion rate values observed ~2 weeks into the eruption [see *Lipman and Banks*, 1987, Table 57.4]. This suggests that the calculated effusion rates for the Ascraeus Mons flow may similarly represent minimum values. Furthermore, effusion rates in terrestrial channeled flows fluctuate. The maximum effusion rate may occur at the eruption onset and then wane with time, or the effusion rate may pulse during the eruption. We suggest that it is unlikely that the Ascraeus Mons flow had a constant effusion rate based on observations of terrestrial flows [e.g., *Lipman and Banks*,

Table 4. Eruption Parameters for Channeled Polyethylene Glycol (PEG) Flows

Flow	Slope, θ (°)	Temperature (Solution), $T_{solution}$ (°C)	Density (Solution), $\rho_{solution}$ (g/cm^3)	Temperature (PEG), T_{wax} (°C)	Effusion Rate, Q (mL/s)	Volume[a], V (mL)	Duration[b], t (s)	Ψ[c]
BG-93	8	12.0	1.1090	24.0	4.5	1300	290	47
BG-96	8	12.5	1.1120	24.0	5.2	1500	289	49
BG-97	8	11.0	1.1180	24.0	5.1	1500	295	15
BG-100	12	10.0	1.1160	24.0	4.7	1700	371	14
BG-101	12	9.5	1.1105	24.0	4.8	1600	339	20

[a]Volumes calculated by multiplying effusion rate and duration.
[b]Duration measured from the initial effusion from vent to the moment wax is cutoff.
[c]Ratio of timescale of solidification to timescale of advection [*Fink and Griffiths*, 1990].

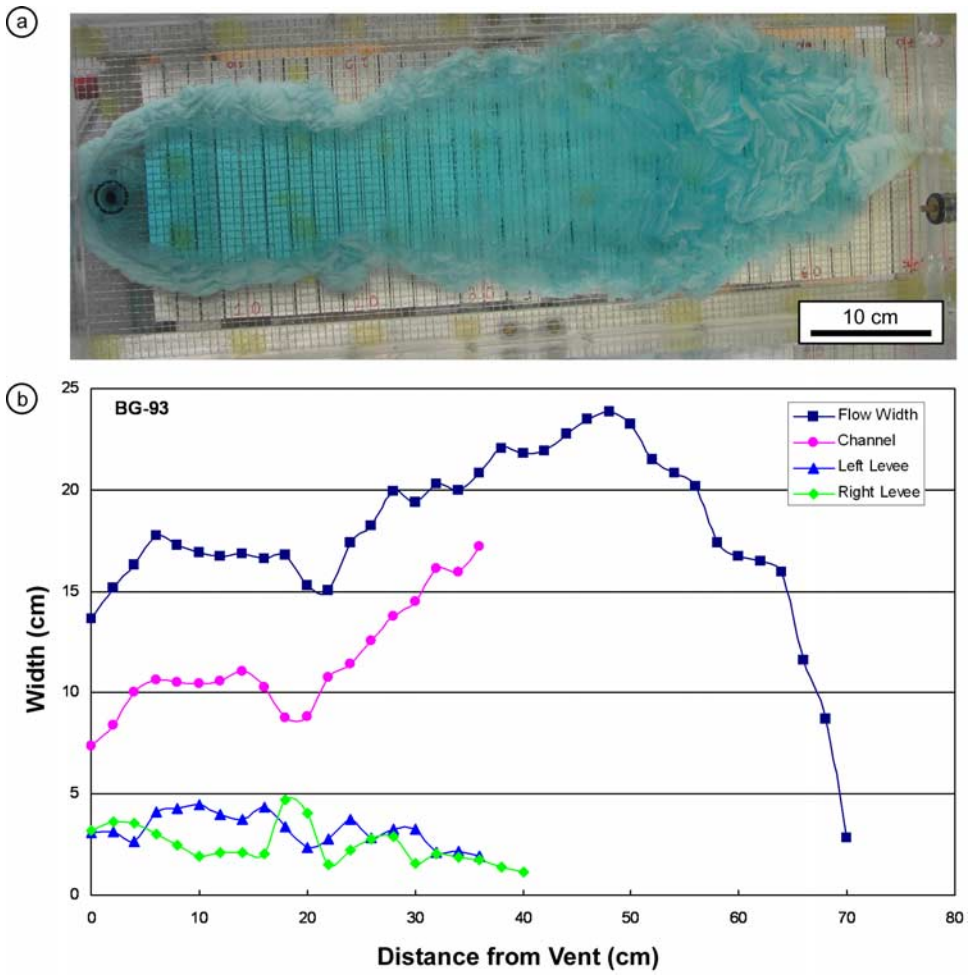

Figure 16. (a) Plan view of a channeled PEG flow: BG-93. Darker color is liquid PEG; lighter color is solid PEG. The vent is located at the left, and the flow direction is to the right. Dark black lines on the bottom of the tank are spaced at 2-cm intervals. Eruption parameters listed in Table 4. (b) Graph of the change in flow, channel, and levee width with distance. Measurements were taken at 2-cm intervals from the image in Figure 16a.

1987]. When we assume a constant effusion rate and continuous eruption, the Ascraeus Mons flow was emplaced in 99 to 223 Earth days, on the basis of effusion rates using equation (3). The short emplacement time of the Ascraeus Mons flow corresponds to channeled terrestrial lava flows which are associated with shorter duration and higher effusion rate eruptions [e.g., *Rowland and Walker*, 1990; *Keszthelyi and Self*, 1998].

4.3. Thermal and Mechanical Erosion in the Proximal Channel

[24] We argue that the observed morphology of the proximal section of the Ascraeus Mons flow may be a product of thermal and mechanical erosion. This section of the flow has no visibly distinct flow margin, but has a measured channel depth of 11–35 m (Table 3). We propose that the eruption began as a thin flow and formed a deeper channel by eroding the channel floor. Teardrop-shaped islands and the nested channel could have formed by either construction or erosion. One observation that supports an erosion origin of the islands (Figure 6a) is a narrow (90–100 m wide) rivulet that crosscuts one of the islands. The rivulet is interpreted to have formed prior to the eruption and was subsequently eroded by the Ascraeus Mons flow, with only a section of it preserved within the channel island. The precise relationship between the primary channel of the Ascraeus Mons flow and narrow rivulets oblique to flow direction cannot be constrained without higher-resolution images.

[25] The nested channel could have formed after a decrease in effusion rate and corresponding lava level within the channel. For example, a cross section of the 1984 Mauna Loa flow shows that a nested channel formed in the late stages of the flow [*Lipman and Banks*, 1987, Figure 57.18 H]. *Lipman and Banks* [1987] also infer erosion of initial base material from the flow as the channel matured. Evidence of thermal erosion in terrestrial flows is observed in basalt flows, but mainly in lava tubes [*Swanson et al.*, 1972; *Greeley et al.*, 1998; *Kauahikaua et al.*, 1998], where the flow is thermally insulated and is sustained for several months. We observed an inner channel along the medial section of the eastern lobe of the 1907 flow (see

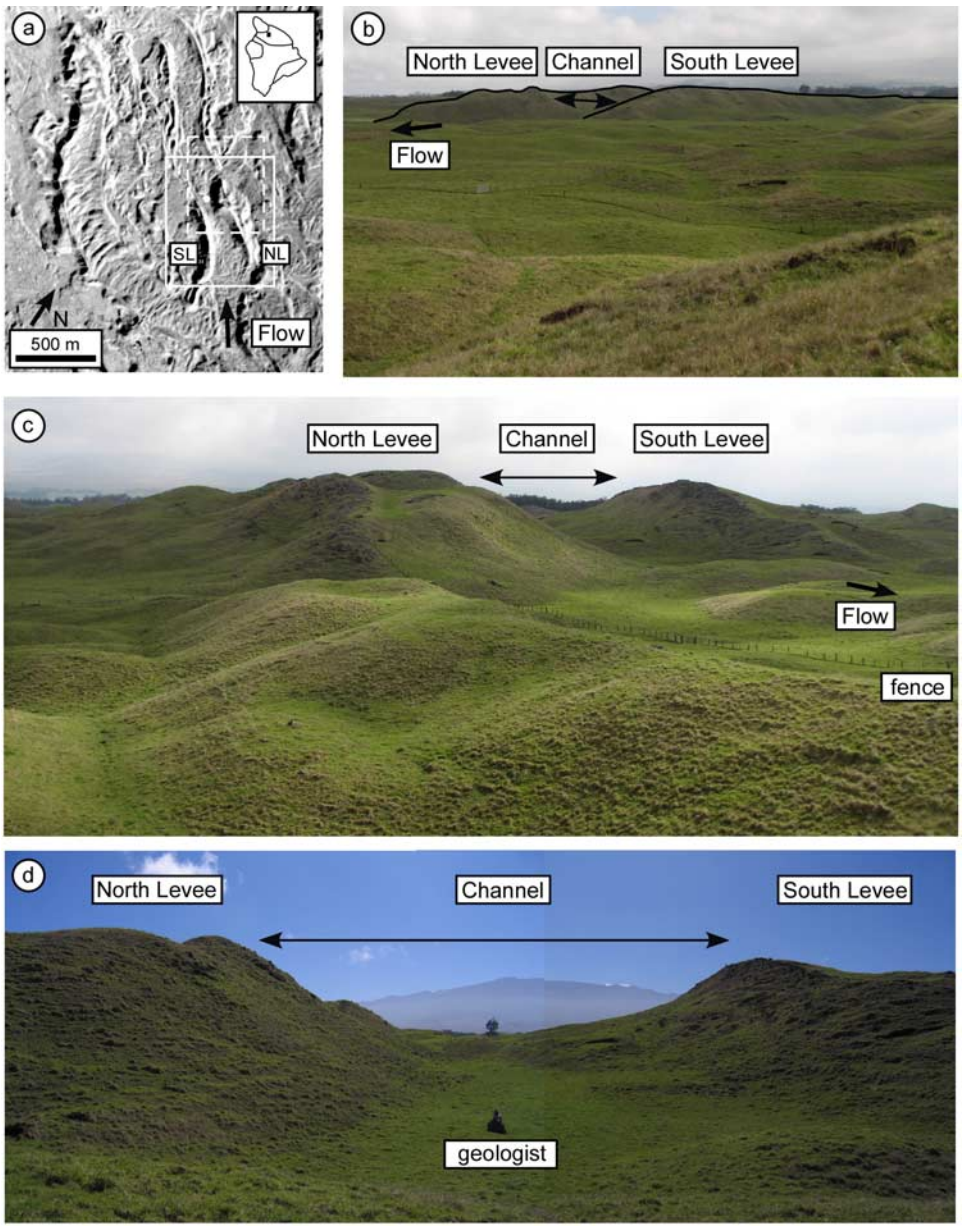

Figure 17. The Mana flow on the north flank of Mauna Kea Volcano, Hawaii. (a) Aerial photo of a portion of the Mana flow field (U.S. Department of Agriculture photograph EKL-8CC-77). Field of view for other images marked by solid white line (Figure 17b) and dashed line (Figure 17c); white dot marks location of geologist in Figure 17d. South levee (SL) and north levee (NL) are also labeled. (b) View of levees from the adjacent channeled flow. (c) Oblique view of levees. Looking upstream. Note fence for scale. (d) Upstream view of the channel and levees. Mauna Kea Volcano is in the background. A geologist is sitting on a rock for scale. Width of channel is ~100 m across. The eastern limb of the Mana flow pictured in Figures 17b, 17c, and 17d is interpreted to have diverted from the western limb (see Figure 17a). The levees of the eastern limb are more prominent, because the majority of the lava drained out of the channel after the eruption ceased, whereas the channel on the western limb remained filled in.

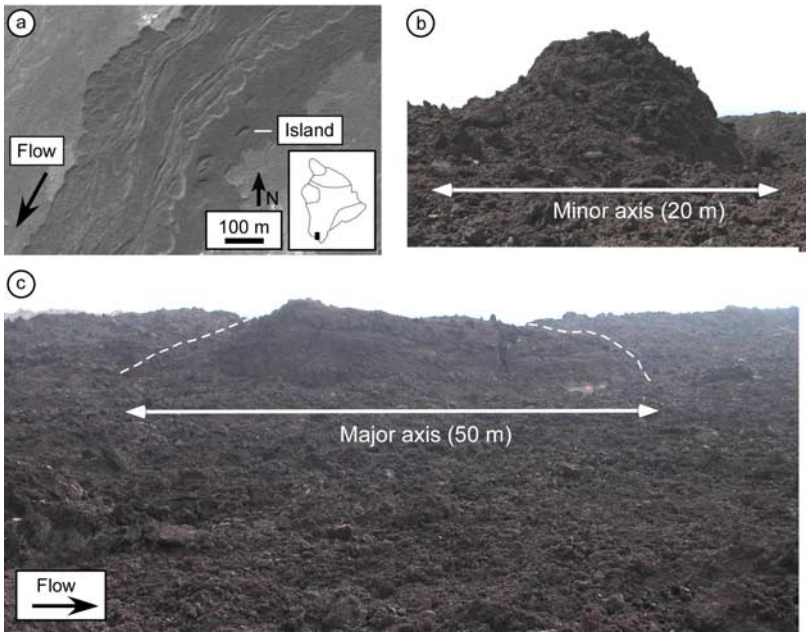

Figure 18. Islands within the channel of the 1907 flow, Mauna Loa Volcano, Hawaii. (a) IKONOS image (1 m/pixel) of part of the 1907 lava flow. Island pictured in (b) and (c) is labeled. Inset marks general location on the big island of Hawaii. (b) Minor axis of the island structure. Looking downstream (south). (c) Major axis of the island structure. Looking east.

profiles 6 and 7, Zimbelman et al., in review), but the inner channel appeared to be a constructional rather than an erosional feature.

4.4. Requirements for a Long Lava Flow on Mars?

[26] Numerous papers have addressed the issue surrounding which factors control the length of lava flows [e.g., *MacDonald*, 1972; *Walker*, 1973; *Malin*, 1980; *Pieri and Baloga*, 1986; *Pinkerton and Wilson*, 1994, *Rowland et al.*, 2005]. Factors presented include viscosity, effusion rate, and erupted volume. Additional considerations were also made of underlying slope, changes in rheologic properties due to crystallization and loss of volatiles, variations in effusion rate, and rate of heat loss with distance. With so many different aspects of the lava flow and the environment to consider, what are the parameters necessary to achieve extraordinary flow lengths? *Keszthelyi and Self* [1998] determined criteria for the development of long lava flows in terrestrial subaerial environments and proposed two primary methods of emplacement as follows: rapid and insulated. Channeled lava flows are inferred to fall under the rapid emplacement category. For a channeled, terrestrial, basaltic flow to reach >100 km, the following physical conditions are needed: effusion rates >200 to 17,000 m^3/s, channel depths >2–19 m, flow velocities 4–12 m/s, low slopes <5°, and cooling of <0.5°C/km [*Keszthelyi and Self*, 1998]. What, then, are the requirements for a flow to reach lengths of hundreds of kilometers on Mars?

[27] We apply the requirements established by *Keszthelyi and Self* [1998] for long terrestrial flows to long lava flows on Mars. Results of numerical models by *Glaze and Baloga* [1998] and *Rowland et al.* [2004] suggest that a lava flow under a given set of eruption conditions would flow a shorter distance on Mars than on Earth. The smaller acceleration due to the gravity on Mars will not only result in a smaller flow velocity, but the amount of cooling over a specific distance will be greater than on Earth, increasing viscosity and producing a thicker flow [*Glaze and Baloga*, 1998]. From these basic assumptions, we can infer that the Ascraeus Mons flow would need to have a higher effusion rate and flow velocity than a hypothetical terrestrial flow of the same length. The range of the effusion rates that we calculated for the Ascraeus Mons flow are greater than those of observed subaerial terrestrial eruptions, but are of the same order of magnitude as the upper values suggested by *Keszthelyi and Self* [1998] necessary to achieve a long lava flow by rapid emplacement. We suggest that, to achieve flows of similar dimensions on Mars and Earth, the effusion rate for the Martian flow must be greater than that of the terrestrial flow because of a slower advance rate

Table 5. Channel Velocity Estimates for the Ascraeus Mons Flow

Density (Lava)[a], ρ_{lava}	Gravitational Acceleration (Mars)[a], g_{Mars}	Slope, θ	Channel Depth, d	Dynamic Viscosity (Lava)[a], η_{lava}	Channel Velocity, v_C	Reynolds Number[b], Re
kg/m^3	m/s^2	°	m	Pa s	m/s	
2000	3.7	0.3	20	1000	5	207
2000	3.7	0.3	30	1000	12	697
2000	3.7	0.3	40	1000	21	1653
2000	3.7	0.3	50	1000	32	3229
2000	3.7	0.3	60	1000	46	5579
2600	3.7	0.3	20	100,000	0.07	0.03
2600	3.7	0.3	30	100,000	0.15	0.12
2600	3.7	0.3	40	100,000	0.27	0.28
2600	3.7	0.3	50	100,000	0.42	0.55
2600	3.7	0.3	60	100,000	0.60	0.94

[a]Values for density and viscosity of the lava are from the works of *Wilson and Mouginis-Mark* [2001] and *Baloga et al.* [2003].
[b]Re < 2000 is considered laminar.

Table 6. Effusion Rate and Emplacement Duration for Ascraeus Mons Flow

Parameter		Units	*A*	B	C
Flow Width	W_F	km	8	8	8
Flow Thickness	H_F	m	40	50	60
Flow Length	L_F	km	690	690	690
Area	A	km^2	6200	6200	6200
Volume[a]	V	km^3	248	310	372
Effusion Rate[b]	Q	m^3/s	28,980	23,184	19,320
Duration[c]	t	days	99	155	223

[a]Volume = area × flow thickness.
[b]From equation (3).
[c]1 day = 24 hours.

due to smaller acceleration due to gravity and the faster cooling rate (temperature decrease per kilometer of flow length) on Mars. This assumes a given underlying slope and initial properties of the lava. Further analysis of the morphology of additional long channeled lava flows on Mars will help to constrain emplacement conditions within the Tharsis region.

5. Summary

[28] We have used the final flow morphology to interpret the emplacement of the 690-km-long Ascraeus Mons flow. The proximal section of this flow is defined by a channel (0.2–2.2 km wide and ≤35 m deep) for 70 km of the flow length, with no distinct flow margin present. The flow thickens (to 30–60 m) in the medial section, and the channel is bounded by well-defined levees and a flow margin. The distal 190 km of the flow is a wide (≤38.6 km) and thick (≤110 m) nonchanneled lobe. Downstream changes in flow morphology are similar to those observed in the 1907 flow on Mauna Loa Volcano and polyethylene glycol (PEG) laboratory simulations. Flow thickness is comparable to that of channeled lava flows on Mauna Kea Volcano, Hawaii, where the levees are ≤35 m thick, but the width dimensions for the Hawaiian flow are narrower than those of the Ascraeus Mons flow. A portion (~48 km long) of the medial section is nonchanneled, which we infer could be due to the roofing of the channel, the remnant lava that stalled and solidified in the channel, or the lava that was blocked by a dam and did not break through. Within the channel are islands which resemble flow structures observed in the 1907 and 1984 flows on Mauna Loa Volcano, Hawaii. The island structures in the terrestrial flows are associated with material that was rafted down by surges of lava and deposited and streamlined by lava that continued to flow past. We suggest that the islands observed in the medial section of the Ascraeus Mons flow may also be deposited and streamlined during surge events. Islands in the proximal section are interpreted to have formed by thermal and mechanical erosion based on cross-cutting relations with local rivulets and the lack of a well-defined flow margin. Channel velocities (0.7 to 46 m/s) and associated Reynolds numbers indicate that the flow style was laminar. We have calculated minimum effusion rates of 19,000–29,000 m^3/s using an application of the Graetz equation. This yields possible eruption durations of 99 to 223 Earth days based on a range of flow volumes for the Ascraeus Mons flow, assuming a constant flow rate and continuous eruption duration. Eruption conditions to achieve long lava flows on Mars are similar to those suggested for terrestrial flows [e.g., *Keszthelyi and Self*, 1998], but Martian flows require greater effusion rates to achieve the same length of a terrestrial flow, assuming a given underlying slope and initial lava properties, because of the smaller acceleration due to the gravity on Mars.

[29] **Acknowledgments.** We thank Malin Space Science Systems (http://www.msss.com/moc_gallery/) and NASA/JPL/Arizona State University (http://themis.asu.edu) for the use of MOC and THEMIS images, respectively. We also thank Barbara Bruno and Lionel Wilson for their reviews, which greatly added to the final paper. Funding for this research was provided by NASA grant NNG04GJ21G from the Planetary Geology and Geophysics Program and Smithsonian Research support. The PEG experiments were funded by NSF OCE-0425073 in a grant to Tracy Gregg.

References

Anderson, J. A., S. C. Sides, D. L. Soltesz, T. L. Sucharski, and K. J. Becker (2004), Modernization of the Integrated Software for Imagers and Spectrometers, 35th Lunar and Planetary Science Conference, Houston, Texas, March 15–19, Abstract 2039.

Anderson, S. W., S. M. Colley, J. H. Fink, and R. K. Hudson (2005), The development of fluid instabilities and preferred pathways in lava flow interiors: Insights from analog experiments and fractal analysis, in *Kinematics and Dynamics of Lava Flows*, Spec. Pap. Geol. Soc. Am., 396, edited by M. Manga and G. Ventura, pp. 147–159, GSA, doi:10.1130/2005.2396(10).

Atkinson, A., T. J. Griffin, and P. J. Stephenson (1975), A major lava tube system from the Undara Volcano, North Queensland, *Bull. Volcanol.*, *39*, 1–28.

Baloga, S. M., P. J. Mouginis-Mark, and L. S. Glaze (2003), Rheology of a long lava flow at Pavonis Mons, Mars, *J. Geophys. Res.*, *108*(E7), 5066, doi:10.1029/2002JE001981.

Barnard, W. M. (1990), *Mauna Loa—A Source Book. Historical Eruptions and Exploration, Volume One: From 1778 Through 1907*, 353 pp., Fredonia, New York.

Barnard, W. M. (1995), Mauna Loa Volcano: Historical eruptions, exploration, and observations (1779–1910), in *Mauna Loa Revealed: Structure, Composition, History, and Hazards, AGU Geophys. Monogr. Ser.*, vol. 92, edited by J. M. Rhodes and J. P. Lockwood, 348 pp., AGU, Washington, D. C.

Blake, S., and B. C. Bruno (2000), Modelling the emplacement of compound lava flows, *Earth Planet. Sci. Lett.*, *184*, 181–197.

Carr, M. H., and R. Greeley (1980), Volcanic features of Hawaii: A basis for comparison with Mars, *NASA SP-403*, 211 pp., US Government Printing Office, Washington, D. C.

Christensen, P. R., et al. (2004), The Thermal Emission Imaging System (THEMIS) for the Mars 2001 Odyssey Mission, *Space Sci. Rev.*, *110*, 85–130.

Christensen, P. R., N. S. Gorelick, G. L. Mehall, and K. C. Murray (2006), *THEMIS Public Data Releases*, Planetary Data System node, Ariz. State Univ., http://themis-data.asu.edu.

Fink, J. H., and R. W. Griffiths (1990), Radial spreading of viscous-gravity currents with solidifying crust, *J. Fluid Mech.*, *221*, 485–509.

Fink, J. H., and J. R. Zimbelman (1990), Longitudinal Variations in rheological properties of lavas: Puu O'o basalt flows, Kilauea volcano, Hawaii, in *Lava Flows and Domes*, edited by J. H. Fink, pp. 157–173, Springer, New York.

Fink, J. H., and R. W. Griffiths (1998), Morphology, eruption rates, and rheology of lava domes: Insights from laboratory models, *J. Geophys. Res.*, *103*(B1), 527–545.

Gaddis, L., et al. (1997), An overview of the Integrated Software for Imaging Spectrometers (ISIS), 28th Lunar and Planetary Science Conference, Abstract 1226.

Garry, W. B. (2006), Emplacement of channeled flows in subaerial, submarine, simulated, and extraterrestrial environments, Ph.D. thesis, 240 pp., SUNY—Univ. at Buffalo, Buffalo, New York, 1 Jun.

Garry, W. B., T. K. P. Gregg, S. A. Soule, and D. J. Fornari (2006), Formation of submarine lava channel textures: Insights from laboratory simulations, *J. Geophys. Res.*, *111*, B03104, doi:10.1029/2005JB003796.

Glaze, L. S., and S. M. Baloga (1998), Dimensions of Pu'u 'O'o lava flows on Mars, *J. Geophys. Res.*, *103*(E6), 13,659–13,666.

Greeley, R. (1987), The role of lava tubes in Hawaiian volcanoes, *U.S. Geol. Surv. Prof. Pap.*, *1350*, 1589–1602.

Greeley, R., S. A. Fagents, R. S. Harris, S. D. Kadel, and D. A. Williams (1998), Erosion by flowing lava: Field evidence, *J. Geophys. Res.*, *103*(B11), 27,325–27,345.

Gregg, T. K. P., and J. H. Fink (1995), Quantification of submarine lava-flow morphology through analog experiments, *Geology*, *23*, 73–76.
Gregg, T. K. P., and J. H. Fink (1996), Quantification of extraterrestrial lava flow effusion rates through laboratory simulations, *J. Geophys. Res.*, *101*, 16,891–16,900.
Gregg, T. K. P., and J. H. Fink (2000), A laboratory investigation into the effects of slope on lava flow morphology, *J. Volcanol. Geotherm. Res.*, *96*, 145–159.
Griffiths, R. W., and J. H. Fink (1992a), Solidification and morphology of submarine lavas: a dependence on extrusion rate, *J. Geophys. Res.*, *97*(B13), 19729–19737.
Griffiths, R. W., and J. H. Fink (1992b), The morphology of lava flows in planetary environments: Predictions from analog experiments, *J. Geophys. Res.*, *97*(B13), 19739–19748.
Griffiths, R. W., and J. H. Fink (1997), Solidifying Bingham extrusions: A model for the growth of silicic lava domes, *J. Fluid Mech.*, *347*, 13–36.
Griffiths, R. W., K. C. Kerr, and K. V. Cashman (2003), Patterns of solidification in channel flows with surface cooling, *J. Fluid Mech.*, *496*, 33–62.
Harris, A. J. L., and S. K. Rowland (2001), FLOWGO: a kinematic thermo-rheological model for lava flowing in a channel, *Bull. Volcanol.*, *63*, 20–44, doi:10.1007/s004450000120.
Hulme, G., and G. Fielder (1977), Effusion rates and rheology of lunar lavas, *Phil. Trans. R. Soc. Lond.*, *A285*, 227–234.
Jeffreys, H. (1925), The flow of water in an inclined channel of rectangular section, *Philos. Mag.*, *49*, 793–807.
Kauahikaua, J., K. V. Cashman, T. N. Mattox, C. C. Heliker, K. A. Hon, M. T. Mangan, and C. R. Thornber (1998), Observations on basaltic lava streams in tubes from Kilauea volcano, island of Hawai'i, *J. Geophys. Res.*, *103*(B11), 27303–27323.
Keszthelyi, L., and S. Self (1998), Some physical requirements for the emplacement of long basaltic lava flows, *J. Geophys. Res.*, *103*(B11), 27447–27464.
Lipman, P. W., and N. G. Banks (1987), 'A'a flow dynamics, *U.S. Geol. Surv. Prof. Pap.*, *1350*, 1527–1567.
Lyman, A. W., E. Koenig, and J. H. Fink (2004), Predicting yield strengths and effusion rates of lava domes from morphology and underlying topography, *J. Volcanol. Geotherm. Res.*, *129*, 125–138.
Macdonald, G. A. (1972), *Volcanoes*, pp. 66–67, Prentice-Hall, Upper Saddle River, N. J.
Macdonald, G. A., and A. T. Abbott (1970), *Volcanoes in the Sea: The Geology of Hawai'i*, 441 pp., The Univ. Press of Hawai'i, Honolulu, Hawaii.
Malin, M. C. (1980), Lengths of Hawaiian lava flows, *Geology*, *8*, 306–308.
Malin, M. C., et al. (1998), Early views of the Martian surface from the Mars Orbiter Camera of Mars Global Surveyor, *Science*, *279*, 1681–1685.
McSween, H. Y., et al. (2006), Alkaline volcanic rocks from the Columbia Hills, Gusev crater, Mars, *J. Geophys. Res.*, *111*, E09S91, doi:10.1029/2006JE002698.
Moore, H. J. (1987), Preliminary estimates of the rheologic properties of 1984 Mauna Loa lava, *U. S. Geol. Surv. Prof. Pap.*, *1350*, 1569–1588.
Mouginis-Mark, P., and M. Tatsumura-Yoshioka (1998), The long lava flows of Elysium Planitia, Mars, *J. Geophys. Res.*, *103*(B11), 19,389–19,400.
Peitersen, M. N., and D. A. Crown (1999), Downflow width behavior of Martian and terrestrial lava flows, *J. Geophys. Res.*, *104*(E4), 8473–8488.
Pieri, D. C., and S. M. Baloga (1986), Eruption rate, area and length relationships for some Hawaiian flows, *J. Volcanol. Geotherm. Res.*, *30*, 29–45.
Pinkerton, H., and R. S. J. Sparks (1976), The 1975 sub-terminal lavas, Mount Etna: A case history of the formation of a compound lava field, *J. Volcanol. Geotherm. Res.*, *1*, 167–182.
Pinkerton, H., and L. Wilson (1994), Factors controlling the lengths of channel-fed lava flows, *Bull. Volcanol.*, *56*, 108–120.
Plescia, J. B. (2004), Morphometric properties of Martian volcanoes, *J. Geophys. Res.*, *109*, E03003, doi:10.1029/2002JE002031.
Roark, J. H., H. V. Frey, and S. E. H. Sakimoto (2000), Interactive graphics tools for analysis of MOLA and other data, 31st Lunar and Planetary Science Conference, Houston, Texas, Abstract 2026.
Rowland, S. K., and G. P. L. Walker (1990), Pahoehoe and 'a'a in Hawai'i: Volumetric flow rate controls the lava structure, *Bull. Volcanol.*, *52*, 615–628.
Rowland, S. K., A. J. L. Harris, and H. Garbeil (2004), Effects of Martian conditions on numerically modeled, cooling-limited, channelized lava flows, *J. Geophys. Res.*, *109*, E10010, doi:10.1029/2004JE002288.
Rowland, S. K., H. Garbeil, and A. J. L. Harris (2005), Lengths and hazards from channel-fed lava flows on Mauna Loa, Hawai'i, determined from thermal and downslope modeling with FLOWGO, *Bull. Volcanol.*, *67*, 634–647, doi:10.1007/s00445-004-0399-x.
Sakimoto, S. E. H., and T. K. P. Gregg (2001), Channeled flow: Analytic solutions, laboratory experiments, and applications to lava flows, *J. Geophys. Res.*, *106*(B5), 8629–8644.
Scott, D. H., G. G. Schaber, and K. L. Tanaka (1981), Map showing lava flows in the southeast part of the Tharsis quadrangle of Mars, *U.S. Geol. Surv. Misc. Map Ser. I-1269 (MC-9-SE)*.
Self, S., T. Thordarson, and L. Keszthelyi (1997), Emplacement of continental flood basalt lava flows, in *Large Igneous Provinces: Continental, Oceanic, and Planetary Flood Volcanism*, *Geophys. Monogr. Ser.*, vol. 100, edited by J. J. Mahoney and M. F. Coffin, pp. 381–410, AGU, Washington, D. C.
Smith, D. E., M. T. Zuber, H. V. Frey, J. B. Garvin, and J. W. Head, et al. (1998), Mars Orbiter Laser Altimeter: Experiment summary after the first year of global mapping of Mars, *J. Geophys. Res.*, *106*(E10), 23,689–23,722.
Swanson, D. A., W. A. Duffield, D. B. Jackson, and D. W. Peterson (1972), The complex filling of Alae Crater, Kilauea Volcano, Hawai'i, *Bull. Volcanol.*, *36*, 105–126.
Thordarson, T., and S. Self (1993), The Laki (Skaftar Fires) and Grimsvotn eruptions in 1783–1785, *Bull. Volcanol.*, *55*, 233–263.
Torson, J. M., and K. J. Becker (1997), ISIS—A software architecture for processing planetary images, 28th Lunar and Planetary Science Conference, Houston, Texas, 1443–1444.
Wadge, G. (1981), The variation of magma discharge during basaltic eruptions, *J. Volcanol. Geotherm. Res.*, *11*, 139–168.
Walker, G. P. L. (1973), Lengths of lava flows, *Philos. Trans. R. Soc. London*, *A274*, 107–118.
Wilson, L., and J. W. Head (1983), A comparison of eruption processes on Earth, Moon, Mars, Io and Venus, *Nature*, *302*, 663–669.
Wilson, L., and P. J. Mouginis-Mark (2001), Estimation of volcanic eruption conditions for a large flank event on Elysium Mons, Mars, *J. Geophys. Res.*, *106*(E9), 20,621–20,628.
Wolfe, E. W., and J. Morris (1996), Geologic map of the island of Hawai'i, *U.S. Geol. Surv. Prof. Pap., Map I-2524-A 1:100,000*.
Zimbelman, J. R. (1985), Estimates of rheologic properties for flows on the Martian volcano Ascraeus Mons, 16th Lunar and Planetary Science Conference, part 1, in J. Geophys. Res., 90, D157–D162.
Zimbelman, J. R. (1998), Emplacement of long lava flows on planetary surfaces, *J. Geophys. Res.*, *103*(B11), 27,503–27,516.

W. B. Garry and J. R. Zimbelman, Center for Earth and Planetary Studies, Smithsonian Institution, PO Box 37012, National Air and Space Museum, MRC 315, Washington, DC 20012–7012, USA. (garryw@si.edu)

T. K. P. Gregg, Department of Geology, University at Buffalo, 876 Natural Science Complex, Buffalo, New York 14260, USA.